Editors' Suggestion

Nonlocal topological electromagnetic phases of matter

Todd Van Mechelen and Zubin Jacob*

Birck Nanotechnology Center and Purdue Quantum Center, Department of Electrical and Computer Engineering, Purdue University, West Lafayette, Indiana 47907, USA

(Received 10 December 2018; revised manuscript received 5 April 2019; published 28 May 2019)

In (2+1)-dimensional materials, nonlocal topological electromagnetic phases are defined as atomic-scale media which host photonic monopoles in the bulk band structure and respect bosonic symmetries (e.g., time reversal $\mathcal{T}^2 = +1$). Additionally, they support topologically protected spin-1 edge states, which are fundamentally different than spin-$\frac{1}{2}$ and pseudo-spin-$\frac{1}{2}$ edge states arising in fermionic and pseudofermionic systems. The striking feature of the edge state is that all electric and magnetic field components vanish at the boundary, in stark contrast to analogs of Jackiw-Rebbi domain wall states. This surprising open boundary solution of Maxwell's equations, dubbed the quantum gyroelectric effect [Phys. Rev. A **98**, 023842 (2018)], is the supersymmetric partner of the topological Dirac edge state where the spinor wave function completely vanishes at the boundary. The defining feature of such phases is the presence of temporal and spatial dispersion in conductivity (the linear response function). In this paper, we generalize these topological electromagnetic phases beyond the continuum approximation to the exact lattice field theory of a periodic atomic crystal. To accomplish this, we put forth the concept of microscopic photonic band structure of solids, analogous to the traditional theory of electronic band structure. Our definition of topological invariants utilizes optical Bloch modes and can be applied to naturally occurring crystalline materials. For the photon propagating within a periodic atomic crystal, our theory shows that besides the Chern invariant $\mathfrak{C} \in \mathbb{Z}$, there are also symmetry-protected topological (SPT) invariants $\nu \in \mathbb{Z}_N$ which are related to the cyclic point group C_N of the crystal $\nu = \mathfrak{C} \mod N$. Due to the rotational symmetries of light $\mathcal{R}(2\pi) = +1$, these SPT phases are manifestly bosonic and behave very differently from their fermionic counterparts $\mathcal{R}(2\pi) = -1$ encountered in conventional condensed-matter systems. Remarkably, the nontrivial bosonic phases $\nu \neq 0$ are determined entirely from rotational (spin-1) eigenvalues of the photon at high-symmetry points in the Brillouin zone. Our work accelerates progress toward the discovery of bosonic phases of matter where the electromagnetic field within an atomic crystal exhibits topological properties.

DOI: 10.1103/PhysRevB.99.205146

I. INTRODUCTION

From a material science standpoint, all known topological phases of matter to date have been characterized by electronic phenomena [1,2]. This is true for both time-reversal broken phases, often called Chern insulators [3–7], and time-reversal unbroken phases, known as topological insulators [8–10]. The signature of time-reversal broken phases is the quantum Hall conductivity $\sigma_{xy} = ne^2/h$, which is quantized in terms of the electronic Chern invariant $n \in \mathbb{Z}$ [11–13], with e being the elementary charge of the electron and h the Planck constant. Only recently has the idea of bosonic Hall conductivity and topological bosonic phases been put forth [14–22].

However, it should be emphasized that the traditional Hall conductivity [23,24] only has topological significance, with respect to the electron, in the static $\omega = 0$ and long-wavelength $k = 0$ limits of the electromagnetic field $\sigma_{xy}(0, 0) = ne^2/h$. At high frequency $\omega \neq 0$ and short wavelength $k \neq 0$, the Hall conductivity $\sigma_{xy}(\omega, \mathbf{k})$ acquires new physical meaning. We have shown that the electromagnetic field itself becomes topological [25–27]. These topological electromagnetic phases of matter depend on the *global* behavior of $\sigma_{xy}(\omega, \mathbf{k})$, over all frequencies and wave vectors.

Like electrons, the signature of electromagnetic Chern phases $\mathfrak{C} \neq 0$ is topologically protected unidirectional (chiral) edge states. Unlike electrons, however, no physical observable (response/correlation function) is topologically quantized as there is no known equivalent for photons. Nevertheless, the origin of topological quantization $\mathfrak{C} \in \mathbb{Z}$ is always a discontinuity in the underlying Berry connection (gauge field [28]) of the eigenmodes. This phenomenon of gauge discontinuity in the *photonic* eigenmodes fundamentally requires nonlocal gyrotropy (Hall conductivity). Nonlocality, or spatial dispersion, is the momentum dependence of optical parameters. If the Hall conductivity changes sign with momentum $\sigma_{xy}(\omega, \mathbf{k}_{\text{crit}}) = 0$, i.e., the handedness changes, the electromagnetic field is topologically nontrivial $\mathfrak{C} \neq 0$. In two dimensions, σ_{xy} behaves as an effective mass [29–31] and this change in sign is the photonic counterpart of the Chern insulator [3–7], where the exact same situation occurs. This intriguing nonlocal behavior leads to a new topological bosonic phase of matter, a quantum gyroelectric phase

*zjacob@purdue.edu

[25–27], which is unlike any known fermionic phase as it is intrinsically tied to the electromagnetic field.

As of yet, only the continuum topological theory of the aforementioned quantum gyroelectric effect has been solved [25–27]. Our goal is to extend this concept beyond the long-wavelength approximation to the exact lattice field theory of optical Bloch waves. In this regime, we must consider not only the first spatial component $\sigma_{xy}(\omega, \mathbf{k}) = \sigma_{xy}(\omega, \mathbf{k}, \mathbf{0})$ but all spatial harmonics of the crystal $\mathbf{g} \neq \mathbf{0}$, to infinite order,

$$J_x^{\text{Hall}}(\omega, \mathbf{k}) = \sum_{\mathbf{g}} \sigma_{xy}(\omega, \mathbf{k}, \mathbf{g}) E_y(\omega, \mathbf{k} + \mathbf{g}). \tag{1}$$

$\mathbf{g} \cdot \mathbf{R} \in 2\pi\mathbb{Z}$ are the reciprocal lattice vectors and $\mathbf{R}$ is the primitive vector of the crystal. In this case, E_i is the *microscopic* electric field. The electromagnetic field must be described to the same scale as the electronic wave functions, i.e., for photon momenta on the order of the lattice constant $ka = \pi$, with $a \approx 5$ Å. Since topological invariants are fundamentally global properties, these astronomically deep subwavelength fields actually play a role in the topological physics.

The idea of lattice topologies in electromagnetism was first proposed by Haldane [32,33] in the context of photonic crystals [34–41]. These are artificial materials composed of two or more different constituents which form a macroscopic crystalline structure. A few important examples are gyrotropic photonic crystals [34–36], Floquet topological insulators [42–44], and bianisotropic metamaterials [45–59]. Instead, we focus on the microscopic domain and utilize the periodicity of the atomic lattice itself. Thus, the topological invariants in our theory are connected to the microscopic atomic lattice and not artificially engineered macroscopic structures. We stress that in the microscopic case, the electromagnetic theory is manifestly bosonic [60–63] (e.g., time reversal $\mathcal{T}^2 = +1$) and characterizes topological phases of matter fundamentally distinct from known fermionic and pseudofermionic phases.

With that in mind, this paper is dedicated to solving two long-standing problems, which is of interest to both photonics and condensed-matter physics. The first, is developing the rigorous theory of optical Bloch modes in natural crystal solids. This problem gained significant interest in the 1960s and 1970s in the context of spatial dispersion (nonlocality) as it led to qualitatively new phenomena, such as natural optical activity (gyrotropy) [64–67]. The current paper builds on our recent discovery of the quantum gyroelectric effect [25–27] where we have shown that nonlocality is also essential for topological phenomena and is a necessary ingredient in any long-wavelength theory. However, since topological field theories are global constructs, a complete picture can only be achieved in the microscopic domain of Bloch waves. Most of the foundations have been summarized by Agronovich and Ginzburg in their seminal monograph on crystal optics [68]. Nevertheless, topological properties have never been tackled to date and a few fundamental quantities, such as the Bloch energy density, have not been defined.

This leads to the second problem—deriving the electromagnetic topological invariants of these systems given only the atomic lattice. We solve this problem and also provide a systematic bosonic classification of all (2+1)-dimensional (2+1D) topological photonic matter. Utilizing the optical Bloch modes, we show that a Chern invariant $\mathfrak{C} \in \mathbb{Z}$ can be found for any two-dimensional crystal and characterizes distinct topological phases. We then go one step further and classify these topological phases with respect to the symmetry group of the crystal—the cyclic point groups C_N. These are known as symmetry-protected topological (SPT) phases [69–80] and the spin of the photon is critical to their definition. The rotational symmetries of light $\mathcal{R}(2\pi) = +1$ impart an intrinsically bosonic nature to these phases, which are fundamentally different than their fermionic counterparts $\mathcal{R}(2\pi) = -1$ encountered in conventional condensed-matter systems. We illustrate this fact by directly comparing SPT bosonic and fermionic phases side-by-side. Our rigorous formalism of microscopic photonic band structure provides an immediate parallel with the traditional theory of electronic band structure in crystal solids.

This paper is organized as follows. In Sec. II we develop the general formalism of 2+1D lattice electromagnetism. First we derive the generalized linear response function, accounting for spatiotemporal dispersion to infinite order in the crystal's spatial harmonics $\mathbf{g}$. Thereafter, we find the equivalent Hamiltonian that governs all light-matter Bloch excitations of the material. In Sec. III we study the discrete rotational symmetries (point groups) of the crystal and the implications on spin-1 quantization [81–86] of the photon. The following Sec. IV discusses the electromagnetic Chern number and its relationship to SPT bosonic phases. The bosonic classification of each phase is related directly to integer quantization of the photon (Table I) and this is compared alongside their fermionic counterparts (Table II). Section V presents our conclusions.

The focus of this paper is 2+1D topological electromagnetic (bosonic) phases of matter $\mathfrak{C} \neq 0$ which requires breaking time-reversal symmetry. These bosonic Chern insulators are ultimately related to nonlocal gyrotropic response (Hall conductivity) and show unidirectional, completely transverse electromagnetic (TEM) edge states [25–27]. However, time-reversal symmetric topological phenomena can arise in higher dimensional systems in the context of nonlocal magnetoelectricity [87]. These time-reversal symmetric phases possess counterpropagating TEM edge states and are interpreted as two copies of a bosonic Chern insulator. Features of topological phenomena, such as spin-momentum locking [88–92], have also been reported in conventional surface state problems: surface plasmon polaritons, Dyakonov waves, etc. However, these traditional surface properties are not connected to any topologically protected edge states or nontrivial phases.

II. LATTICE ELECTROMAGNETISM

A. 2+1D electrodynamics

In this paper we focus on two-dimensional materials and the topological electromagnetic phases associated with them. The preliminaries for 2+1D electromagnetism can be found in Appendix A of Ref. [25]. Conveniently, the restriction to 2D limits the degrees of freedom of both the electromagnetic field and the induced response of the material, such that strictly transverse-magnetic (TM) waves propagate. The correspond-

TABLE I. Summary of 2+1D topological electromagnetic (bosonic) phases. Symmetry-protected topological (SPT) bosonic phases exist in all cyclic point groups $C_{N=2,3,4,6}$. The continuous group C_∞ describes the long-wavelength theory $k \approx 0$. The topological phases are characterized by their Chern invariant $\mathfrak{C} \in \mathbb{Z}$ and SPT invariant $\nu \in \mathbb{Z}_N$. These numbers are not independent, but intimately related by the symmetries of the crystal: $\nu = \mathfrak{C} \mod N$. ν is protected by N-fold rotational symmetry and determines the Chern number up to a factor of N. The bosonic classification of ν represents the direct product of rotational eigenvalues $(\eta_N)^N = +1$ (roots of unity) of the electromagnetic field at high-symmetry points (HSPs) in the Brillouin zone. For the spin-1 photon, this classification is more intuitively understood in terms of modulo integers $m_N \in \mathbb{Z}_N$, which determine the N possible eigenvalues of $\eta_N = \exp[i\frac{2\pi}{N}m_N]$.

Point group, C_N	Symmetry, $\mathbb{Z}_N$	Bosonic classification, $(\eta_N)^N = +1$	Boson SPT invariant, $\nu = \mathfrak{C} \mod N$
C_1			
C_2	$\mathbb{Z}_2$	$\exp(i2\pi\mathfrak{C}/2) = \eta_2(\Gamma)\eta_2(X)\eta_2(Y)\eta_2(M)$	$\nu = m_2(\Gamma) + m_2(X) + m_2(Y) + m_2(M) \mod 2$
C_3	$\mathbb{Z}_3$	$\exp(i2\pi\mathfrak{C}/3) = \eta_3(\Gamma)\eta_3(K)\eta_3(K')$	$\nu = m_3(\Gamma) + m_3(K) + m_3(K') \mod 3$
C_4	$\mathbb{Z}_4$	$\exp(i2\pi\mathfrak{C}/4) = \eta_4(\Gamma)\eta_4(M)\eta_2(Y)$	$\nu = m_4(\Gamma) + m_4(M) + 2m_2(Y) \mod 4$
C_6	$\mathbb{Z}_6$	$\exp(i2\pi\mathfrak{C}/6) = \eta_6(\Gamma)\eta_3(K)\eta_2(M)$	$\nu = m_6(\Gamma) + 2m_3(K) + 3m_2(M) \mod 6$
C_∞	$\mathbb{Z}$	$\exp(i\theta\mathfrak{C}) = \eta_\theta(0)\eta_\theta^*(\infty), \ \eta_\theta = \exp(i\theta m)$	$\nu = \mathfrak{C} = m(0) - m(\infty)$

ing wave equation reads

$$\mathcal{H}_0 f = i\partial_t g, \quad f = \begin{bmatrix} E_x \\ E_y \\ H_z \end{bmatrix}, \quad g = \begin{bmatrix} D_x \\ D_y \\ B_z \end{bmatrix}. \tag{2}$$

f is the TM polarization state of the electromagnetic field and the material response is captured by the displacement field g. $\mathcal{H}_0(\mathbf{p}) = \mathbf{p}\cdot\mathbf{S}$ are the vacuum Maxwell equations in real space and describe the dynamics of the free photon,

$$\mathcal{H}_0(\mathbf{p}) = p_x\hat{S}_x + p_y\hat{S}_y = \begin{bmatrix} 0 & 0 & -p_y \\ 0 & 0 & p_x \\ -p_y & p_x & 0 \end{bmatrix}. \tag{3}$$

$\mathbf{p} = -i\nabla$ is the two-dimensional momentum operator. $\hat{S}_x$ and $\hat{S}_y$ are spin-1 operators that satisfy the angular momentum algebra $[\hat{S}_i, \hat{S}_j] = i\epsilon_{ijk}\hat{S}_k$,

$$\hat{S}_z = \begin{bmatrix} 0 & -i & 0 \\ i & 0 & 0 \\ 0 & 0 & 0 \end{bmatrix}. \tag{4}$$

Here, $(\hat{S}_z)_{ij} = -i\epsilon_{ijz}$ is the generator of rotations in the x-y plane and is represented by the antisymmetric matrix. In two dimensions, $\hat{S}_z$ governs all rotational symmetries of the electromagnetic field.

B. 2+1D linear response theory

The effective electromagnetic properties of a material are very accurately described by a linear response theory, assuming nonlinear interactions are negligible. This is true for low-intensity light $|f| \lessapprox 10^8$ V/m that is sufficiently weak compared to the atomic fields governing the binding of the crystal itself. Our goal is to characterize the topological field theory in this regime. With this in mind, the most general linear response of a 2D material is nonlocal in both space and time coordinates,

$$g(t, \mathbf{r}) = \int d^2\mathbf{r}' \int_{-\infty}^{t} dt' \mathcal{M}(t, t', \mathbf{r}, \mathbf{r}') f(t', \mathbf{r}'). \tag{5}$$

$\mathcal{M}$ is the response function and compactly represents the constitutive relations in space-time,

$$\mathcal{M}(t, t', \mathbf{r}, \mathbf{r}') = \begin{bmatrix} \varepsilon_{xx} & \varepsilon_{xy} & \chi_x \\ \varepsilon_{yx} & \varepsilon_{yy} & \chi_y \\ \zeta_x & \zeta_y & \mu \end{bmatrix}. \tag{6}$$

Note that $\mathcal{M}$ is a (3×3)-dimensional matrix and we include all possible material responses as a generalization; for instance, magnetism μ and magnetoelectricity χ_i, ζ_i.

If the properties of the crystal are not changing temporally (no external modulation), the response function is translation-

TABLE II. Summary of 2+1D SPT fermionic phases for comparison. The fermionic classification of ν represents the direct product of rotational eigenvalues $(\zeta_N)^N = -1$ (roots of negative unity) of the spinor field at HSPs in the Brillouin zone. For the spin-$\frac{1}{2}$ electron, this classification is more intuitively understood in terms of modulo half-integers $m_N \in \mathbb{Z}_N + \frac{1}{2}$, which determine the N possible eigenvalues of $\zeta_N = \exp[i\frac{2\pi}{N}m_N]$.

Point group, C_N	Symmetry, $\mathbb{Z}_N$	Fermionic classification, $(\zeta_N)^N = -1$	Fermion SPT invariant, $\nu = \mathfrak{C} \mod N$
C_1			
C_2	$\mathbb{Z}_2$	$\exp(i2\pi\mathfrak{C}/2) = \zeta_2(\Gamma)\zeta_2(X)\zeta_2(Y)\zeta_2(M)$	$\nu = m_2(\Gamma) + m_2(X) + m_2(Y) + m_2(M) \mod 2$
C_3	$\mathbb{Z}_3$	$\exp(i2\pi\mathfrak{C}/3) = -\zeta_3(\Gamma)\zeta_3(K)\zeta_3(K')$	$\nu = m_3(\Gamma) + m_3(K) + m_3(K') + \frac{3}{2} \mod 3$
C_4	$\mathbb{Z}_4$	$\exp(i2\pi\mathfrak{C}/4) = -\zeta_4(\Gamma)\zeta_4(M)\zeta_2(Y)$	$\nu = m_4(\Gamma) + m_4(M) + 2m_2(Y) + 2 \mod 4$
C_6	$\mathbb{Z}_6$	$\exp(i2\pi\mathfrak{C}/6) = -\zeta_6(\Gamma)\zeta_3(K)\zeta_2(M)$	$\nu = m_6(\Gamma) + 2m_3(K) + 3m_2(M) + 3 \mod 6$
C_∞	$\mathbb{Z}$	$\exp(i\theta\mathfrak{C}) = \zeta_\theta(0)\zeta_\theta^*(\infty), \ \zeta_\theta = \exp(i\theta m)$	$\nu = \mathfrak{C} = m(0) - m(\infty)$

ally invariant in time,

$$\mathcal{M}(t,t',\mathbf{r},\mathbf{r}') = \mathcal{M}(t-t',\mathbf{r},\mathbf{r}') = \int d\omega\, \mathcal{M}(\omega,\mathbf{r},\mathbf{r}')e^{-i\omega(t-t')}. \tag{7}$$

Equation (7) implies energy conservation in Hermitian systems $\omega' = \omega$. However, a crystal is not translationally invariant in space; momentum is not conserved $\mathbf{k}' \neq \mathbf{k}$. Instead, the crystal is periodic and possesses *discrete* translational symmetry [68,93],

$$\mathcal{M}(\omega,\mathbf{r},\mathbf{r}') = \mathcal{M}(\omega,\mathbf{r}+\mathbf{R},\mathbf{r}'+\mathbf{R}), \tag{8}$$

where $\mathbf{R}$ is the primitive lattice vector of the crystal. This admits a Fourier decomposition in the spatial harmonics of the crystal $\mathbf{g}$,

$$\mathcal{M}(\omega,\mathbf{r},\mathbf{r}') = \sum_{\mathbf{g}} \mathcal{M}_{\mathbf{g}}(\omega,\mathbf{r}-\mathbf{r}')e^{-i\mathbf{r}'\cdot\mathbf{g}}, \tag{9}$$

with $\mathbf{g}\cdot\mathbf{R} \in 2\pi\,\mathbb{Z}$ arbitrary integer combinations of the reciprocal lattice vectors.

Due to nonlocality, it is necessary to convert to the reciprocal space,

$$\mathcal{M}(\omega,\mathbf{k},\mathbf{k}') = \frac{1}{(2\pi)^2}\iint d^2\mathbf{r}\, d^2\mathbf{r}'\mathcal{M}(\omega,\mathbf{r},\mathbf{r}')e^{-i\mathbf{k}\cdot\mathbf{r}}e^{i\mathbf{k}'\cdot\mathbf{r}'}. \tag{10}$$

$\mathcal{M}(\omega,\mathbf{k},\mathbf{k}')$ determines the linear transformation properties of an input wave with momentum $\mathbf{k}'$ to an output wave with momentum $\mathbf{k}$. In a periodic crystal, the momentum is conserved up to a reciprocal vector $\mathbf{k}' = \mathbf{k}+\mathbf{g}$ and represents a discrete spectrum,

$$\mathcal{M}(\omega,\mathbf{k},\mathbf{k}') = \sum_{\mathbf{g}} \mathcal{M}_{\mathbf{g}}(\omega,\mathbf{k})\delta^2(\mathbf{k}+\mathbf{g}-\mathbf{k}'), \tag{11}$$

where $\mathcal{M}_{\mathbf{g}}(\omega,\mathbf{k})$ is the Fourier transformed function with respect to $\bar{\mathbf{r}} = \mathbf{r}-\mathbf{r}'$,

$$\mathcal{M}_{\mathbf{g}}(\omega,\mathbf{k}) = \int d^2\bar{\mathbf{r}}\, \mathcal{M}_{\mathbf{g}}(\omega,\bar{\mathbf{r}})e^{-i\mathbf{k}\cdot\bar{\mathbf{r}}}. \tag{12}$$

$\delta^2(\mathbf{k}+\mathbf{g}-\mathbf{k}')$ is the momentum-conserving delta function. Each Fourier element of the response function $\mathcal{M}_{\mathbf{g}}(\omega,\mathbf{k})$ determines the polarization-dependent scattering amplitude from $\mathbf{k}+\mathbf{g}\to\mathbf{k}$. These are essentially the photonic structure factors of the two-dimensional crystal.

In this case, $\mathbf{k}$ is the crystal momentum and is only uniquely defined within the first Brillouin zone (BZ). Hence, the electromagnetic eigenstates of the medium are Bloch waves,

$$\mathcal{H}_0(\mathbf{k})f_{\mathbf{k}} = \omega\int d^2\mathbf{k}'\mathcal{M}(\omega,\mathbf{k},\mathbf{k}')f_{\mathbf{k}'} = \omega\sum_{\mathbf{g}}\mathcal{M}_{\mathbf{g}}(\omega,\mathbf{k})f_{\mathbf{k}+\mathbf{g}}. \tag{13}$$

$\mathcal{H}_0(\mathbf{k}) = \mathbf{k}\cdot\mathbf{S}$ are the vacuum Maxwell equations in momentum space. The Bloch photonic wave function $\tilde{f}_{\mathbf{k}}(\mathbf{r})$ corresponds to the net propagation of all $\mathbf{k}+\mathbf{g}$ scattered waves in the medium,

$$\tilde{f}_{\mathbf{k}}(\mathbf{r}) = \frac{1}{\sqrt{V}}\sum_{\mathbf{g}} f_{\mathbf{k}+\mathbf{g}}e^{i\mathbf{g}\cdot\mathbf{r}}, \tag{14}$$

where $\tilde{f}_{\mathbf{k}}(\mathbf{r}+\mathbf{R}) = \tilde{f}_{\mathbf{k}}(\mathbf{r})$ is periodic in the atomic crystal lattice and we have normalized by the unit cell area V. For clarity, we use tildes to identify cell-periodic Bloch functions. $f_{\mathbf{k}+\mathbf{g}}$ are the collection of Fourier coefficients associated with each Bloch wave. Note that Eqs. (13) and (14) reduce to the continuum theory [25–27] when considering only the zeroth-order harmonic $\mathbf{g} = \mathbf{0}$.

C. Generalized response function

Nevertheless, Eq. (13) poses a few serious problems; it does not represent a proper first-order in time Hamiltonian since all harmonics of the response function $\mathcal{M}_{\mathbf{g}}(\omega,\mathbf{k})$ depend on the eigenvalue ω. Moreover, it is not evident that the Bloch waves in Eq. (14) are normalizable, as the system contains complex spatial and temporal dispersion. Due to these issues, it is advantageous to return to the more general form of $\mathcal{M}(\omega,\mathbf{k},\mathbf{k}')$ without assuming discrete translational symmetry. This will allow us to derive very robust properties of the response function that can also be applied to amorphous materials or quasicrystals.

First, we demand Hermiticity,

$$\mathcal{M}(\omega,\mathbf{k},\mathbf{k}') = \mathcal{M}^{\dagger}(\omega,\mathbf{k}',\mathbf{k}), \tag{15}$$

such that the response is lossless. To account for normalizable electromagnetic waves, the energy density must be positive definite for all ω,

$$U(\omega) = \iint d^2\mathbf{k}\, d^2\mathbf{k}' f_{\mathbf{k}}^{\dagger}\bar{\mathcal{M}}(\omega,\mathbf{k},\mathbf{k}')f_{\mathbf{k}'} > 0, \tag{16}$$

where $\bar{\mathcal{M}}$ describes the inner product space in a dispersive medium,

$$\bar{\mathcal{M}}(\omega,\mathbf{k},\mathbf{k}') = \frac{\partial}{\partial\omega}[\omega\mathcal{M}(\omega,\mathbf{k},\mathbf{k}')]. \tag{17}$$

Notice that $U(\omega) = U^*(\omega)$ is only real-valued when $\mathcal{M}$ is Hermitian. For realistic materials, the energy density is also stable at static equilibrium $\omega = 0$,

$$U(0) = \iint d^2\mathbf{k}\, d^2\mathbf{k}' f_{\mathbf{k}}^{\dagger}\mathcal{M}(0,\mathbf{k},\mathbf{k}')f_{\mathbf{k}'} > 0, \tag{18}$$

with $\mathcal{M}(0,\mathbf{k},\mathbf{k}') = \bar{\mathcal{M}}(0,\mathbf{k},\mathbf{k}')$ at zero frequency. Stability implies the response function is nonsingular at $\omega = 0$, such that there is a smooth transition to the electrostatic limit $\lim_{\omega\to 0}\omega\mathcal{M}(\omega,\mathbf{k},\mathbf{k}') \to 0$. All dielectric (insulating) materials satisfy this constraint since the induced current arises strictly from time-varying polarizations $J_i = \dot{P}_i + \epsilon_{ij}\partial^j M_z$. By relaxing the stability condition [Eq. (18)], metallic (plasmonic) models can be easily included with slight modifications to $\mathcal{M}$. Metallic materials are singular (unstable) at $\omega = 0$ as they possess dc (static) currents. However, the main focus of this paper is the ground state of dielectric (insulating) materials so we assume the response function is well-behaved around $\omega = 0$.

To ensure the electromagnetic field is real-valued, i.e., represents a neutral particle, we always require the reality

condition,

$$\mathcal{M}(\omega, \mathbf{k}, \mathbf{k}') = \mathcal{M}^*(-\omega, -\mathbf{k}, -\mathbf{k}'). \tag{19}$$

Furthermore, the response is transparent at high frequency $\omega \to \infty$, as the material cannot respond to sufficiently fast temporal oscillations,

$$\lim_{\omega\to\infty} \mathcal{M}(\omega, \mathbf{k}, \mathbf{k}') = \mathbb{1}_3 \delta^2_{\mathbf{k}-\mathbf{k}'}. \tag{20}$$

$\mathbb{1}_3$ is the 3×3 identity matrix and $\delta^2_{\mathbf{k}-\mathbf{k}'} = \delta^2(\mathbf{k} - \mathbf{k}')$ is the momentum-conserving delta function. Lastly, the response must be causal and satisfy the Kramers-Kronig relations,

$$\oint_{\Im[\omega']\geqslant 0} \frac{\mathcal{M}(\omega', \mathbf{k}, \mathbf{k}') - \mathbb{1}_3 \delta^2_{\mathbf{k}-\mathbf{k}'}}{\omega' - \omega} d\omega' = 0. \tag{21}$$

This ensures the response function is analytic in the upper complex plane and decays at least as fast as $|\omega|^{-1}$.

Combining all the above criteria, we find that $\mathcal{M}$ can always be expanded via a partial fraction decomposition,

$$\mathcal{M}(\omega, \mathbf{k}, \mathbf{k}') = \mathbb{1}_3 \delta^2_{\mathbf{k}-\mathbf{k}'} - \sum_\alpha \int d^2\mathbf{k}'' \frac{\mathcal{C}^\dagger_{\alpha\mathbf{k}''\mathbf{k}} \mathcal{C}_{\alpha\mathbf{k}''\mathbf{k}'}}{\omega_{\alpha\mathbf{k}''}(\omega - \omega_{\alpha\mathbf{k}''})}. \tag{22}$$

Any Hermitian (lossless) response function can be expressed in this form. Equation (22) is easily extended to 3D materials but our focus is 2D topological field theories. $\omega_{\alpha\mathbf{k}}$ is the resonant energy of the oscillator and corresponds to a first-order (real-valued) pole of the response function. Note, to satisfy the reality condition [Eq. (19)], each oscillator $\omega_{\alpha\mathbf{k}}$ must always come in pairs with a negative energy resonance $-\omega_{\alpha-\mathbf{k}}$, which we assume is captured by the summation over α.

In this case, α labels an arbitrary bosonic excitation in the material, such as an exciton or phonon, which couples linearly to the electromagnetic fields via the tensor,

$$\mathcal{C}_\alpha(\mathbf{k}, \mathbf{k}') = \frac{1}{(2\pi)^2} \iint d^2\mathbf{r}\, d^2\mathbf{r}' \mathcal{C}_\alpha(\mathbf{r}, \mathbf{r}') e^{-i\mathbf{k}\cdot\mathbf{r}} e^{i\mathbf{k}'\cdot\mathbf{r}'}. \tag{23}$$

In the general case, $\text{rank}[\mathcal{C}_\alpha] = 3$ couples to both the electric field E_i and magnetic field H_z. Pure electric excitations only contribute to the permittivity tensor $\text{rank}[\mathcal{C}_\alpha] = 2$ and couple strictly to the electric field E_i. Likewise, pure magnetic excitations only contribute to the scalar permeability $\text{rank}[\mathcal{C}_\alpha] = 1$ and couple strictly to the magnetic field H_z. All such excitations are accounted for simply by specifying the rank of $\mathcal{C}_\alpha$.

Substituting Eq. (22) into Eq. (16), we can exchange the order of integration $U(\omega) = \int d^2\mathbf{k}\, U(\omega, \mathbf{k})$ and define

$$U(\omega, \mathbf{k}) = |f_\mathbf{k}|^2 + \sum_\alpha \left| \int d^2\mathbf{k}' \frac{\mathcal{C}_{\alpha\mathbf{k}\mathbf{k}'} f_{\mathbf{k}'}}{(\omega - \omega_{\alpha\mathbf{k}})} \right|^2 > 0, \tag{24}$$

which is positive definite for all ω and $\mathbf{k}$. Equation (24) is the generalized inner product for the electromagnetic field and represents the energy density at an arbitrary frequency and wave vector. We will now show that Eq. (22) is derived from a first-order in time Hamiltonian.

D. Generalized Hamiltonian

To find the corresponding Hamiltonian, we expand the response function $\mathcal{M}$ in terms of three-component matter oscillators ψ_α. Similar to a Lorentz oscillator [94], these describe the internal polarization and magnetization modes of the material,

$$\omega\psi_{\alpha\mathbf{k}} = \omega_{\alpha\mathbf{k}}\psi_{\alpha\mathbf{k}} + \int d^2\mathbf{k}' \mathcal{C}_{\alpha\mathbf{k}\mathbf{k}'} f_{\mathbf{k}'}. \tag{25}$$

Substituting Eq. (25) and (22) into Eq. (13) we obtain

$$\begin{aligned}\omega f_\mathbf{k} = \mathcal{H}_0(\mathbf{k}) f_\mathbf{k} &+ \sum_\alpha \iint \frac{d^2\mathbf{k}'' d^2\mathbf{k}'}{\omega_{\alpha\mathbf{k}''}} \mathcal{C}^\dagger_{\alpha\mathbf{k}''\mathbf{k}} \mathcal{C}_{\alpha\mathbf{k}''\mathbf{k}'} f_{\mathbf{k}'} \\ &+ \sum_\alpha \int d^2\mathbf{k}' \mathcal{C}^\dagger_{\alpha\mathbf{k}'\mathbf{k}} \psi_{\alpha\mathbf{k}'}.\end{aligned} \tag{26}$$

The first two terms on the right-hand side of Eq. (26) represent the vacuum equations and self-energy of the electromagnetic field. The third term is the linear coupling to the oscillators. Combining Eqs. (25) and (26) into a single algebraic matrix, we write the generalized Hamiltonian $H(\mathbf{k}, \mathbf{k}')$ as

$$H(\mathbf{k}, \mathbf{k}') = \begin{bmatrix} \mathcal{H}_0(\mathbf{k})\delta^2_{\mathbf{k}-\mathbf{k}'} + \sum_\alpha \int \frac{d^2\mathbf{k}''}{\omega_{\alpha\mathbf{k}''}} \mathcal{C}^\dagger_{\alpha\mathbf{k}''\mathbf{k}} \mathcal{C}_{\alpha\mathbf{k}''\mathbf{k}'} & \mathcal{C}^\dagger_{1\mathbf{k}'\mathbf{k}} & \mathcal{C}^\dagger_{2\mathbf{k}'\mathbf{k}} & \cdots \\ \mathcal{C}_{1\mathbf{k}\mathbf{k}'} & \omega_{1\mathbf{k}}\delta^2_{\mathbf{k}-\mathbf{k}'} & 0 & \cdots \\ \mathcal{C}_{2\mathbf{k}\mathbf{k}'} & 0 & \omega_{2\mathbf{k}}\delta^2_{\mathbf{k}-\mathbf{k}'} & \cdots \\ \vdots & \vdots & \vdots & \ddots \end{bmatrix}, \tag{27}$$

which is manifestly Hermitian $H(\mathbf{k}, \mathbf{k}') = H^\dagger(\mathbf{k}', \mathbf{k})$. The dimension of the Hamiltonian is determined by the rank of all the coupling matrices $\dim[H] = N = 3 + \sum_\alpha \text{rank}[\mathcal{C}_\alpha]$.

We now define $u_\mathbf{k}$ as the generalized state vector of the electromagnetic problem; accounting for the photon $f_\mathbf{k}$ and all possible internal excitations $\psi_{\alpha\mathbf{k}}$,

$$\int d^2\mathbf{k}' H_{\mathbf{k}\mathbf{k}'} u_{\mathbf{k}'} = \omega u_\mathbf{k}, \quad u_\mathbf{k} = \begin{bmatrix} f_\mathbf{k} \\ \psi_{1\mathbf{k}} \\ \psi_{2\mathbf{k}} \\ \vdots \end{bmatrix}, \tag{28}$$

which is a first-order wave equation. Notice that contraction of $u_\mathbf{k}$ naturally reproduces the energy density [Eq. (24)] upon

summation over all degrees of freedom,

$$u_{\mathbf{k}}^{\dagger}u_{\mathbf{k}} = |f_{\mathbf{k}}|^2 + \sum_{\alpha} |\psi_{\alpha\mathbf{k}}|^2 = U(\omega,\mathbf{k}) = |f_{\mathbf{k}}|^2 + \sum_{\alpha} \left| \int d^2\mathbf{k}' \frac{\mathcal{C}_{\alpha\mathbf{k}\mathbf{k}'} f_{\mathbf{k}'}}{(\omega - \omega_{\alpha\mathbf{k}})} \right|^2. \tag{29}$$

The complete set of eigenvectors and eigenvalues is represented by $u_{\mathbf{k}}$. We must define all relevant electromagnetic quantities in terms of this generalized state vector.

E. Crystal Hamiltonian

We are now ready to enforce crystal periodicity. Instead of expanding $\mathcal{M}$ directly, we utilize the periodicity of the coupling tensors $\mathcal{C}_{\alpha}(\mathbf{r},\mathbf{r}') = \mathcal{C}_{\alpha}(\mathbf{r}+\mathbf{R},\mathbf{r}'+\mathbf{R})$, which is a discrete spectrum in $\mathbf{g}$,

$$\mathcal{C}_{\alpha}(\mathbf{r},\mathbf{r}') = \sum_{\mathbf{g}} \mathcal{C}_{\alpha\mathbf{g}}(\mathbf{r}-\mathbf{r}') e^{-i\mathbf{r}'\cdot\mathbf{g}}. \tag{30}$$

After Fourier transforming, we obtain the components in the momentum space,

$$\mathcal{C}_{\alpha}(\mathbf{k},\mathbf{k}') = \sum_{\mathbf{g}} \mathcal{C}_{\alpha\mathbf{g}}(\mathbf{k}) \delta^2(\mathbf{k}+\mathbf{g}-\mathbf{k}'), \tag{31}$$

with respect to $\bar{\mathbf{r}} = \mathbf{r} - \mathbf{r}'$,

$$\mathcal{C}_{\alpha\mathbf{g}}(\mathbf{k}) = \int d^2\bar{\mathbf{r}}\, \mathcal{C}_{\alpha\mathbf{g}}(\bar{\mathbf{r}}) e^{-i\mathbf{k}\cdot\bar{\mathbf{r}}}. \tag{32}$$

$\mathcal{C}_{\alpha\mathbf{g}}(\mathbf{k})$ tells us the scattering amplitude of a photon $f_{\mathbf{k}+\mathbf{g}}$ with momentum $\mathbf{k}+\mathbf{g}$ into an internal mode of the material $\psi_{\alpha\mathbf{k}}$ at momentum $\mathbf{k}$, and vice versa. The crystal Hamiltonian accounts for all such scattering events,

$$H(\mathbf{k},\mathbf{k}') = \sum_{\mathbf{g}} H_{\mathbf{g}}(\mathbf{k}) \delta^2(\mathbf{k}+\mathbf{g}-\mathbf{k}'), \tag{33}$$

with Hermiticity $H_{\mathbf{g}}(\mathbf{k}) = H_{-\mathbf{g}}^{\dagger}(\mathbf{k}+\mathbf{g})$ satisfied by definition.

The quasiparticle eigenstates of the Hamiltonian describe the complete spectrum of Bloch waves,

$$\sum_{\mathbf{g}} H_{\mathbf{g}}(\mathbf{k}) u_{n\mathbf{k}+\mathbf{g}} = \omega_{n\mathbf{k}} u_{n\mathbf{k}}, \tag{34}$$

and the eigenenergies $\omega_{n\mathbf{k}+\mathbf{g}} = \omega_{n\mathbf{k}}$ are periodic Bloch bands. Note, it is important not to confuse the polaritonic eigenenergies $\omega_{n\mathbf{k}}$ with the oscillator energies $\omega_{\alpha\mathbf{k}}$. The eigenenergies $\omega_{n\mathbf{k}}$ constitute modes of the coupled light-matter system while $\omega_{\alpha\mathbf{k}}$ describe the natural matter oscillations in the absence of the electromagnetic field. n labels a particular polaritonic energy band of the material with its associated Bloch eigenstate $\tilde{u}_{n\mathbf{k}}(\mathbf{r})$. The total wave function $\tilde{u}_{n\mathbf{k}}(\mathbf{r})$ contains the photon $\tilde{f}_{n\mathbf{k}}(\mathbf{r})$ and all internal degrees of freedom describing the linear response $\tilde{\psi}_{n\alpha\mathbf{k}}(\mathbf{r})$. This is expressed compactly in the Fourier basis,

$$\tilde{u}_{n\mathbf{k}}(\mathbf{r}) = \frac{1}{\sqrt{V}} \sum_{\mathbf{g}} u_{n\mathbf{k}+\mathbf{g}} e^{i\mathbf{g}\cdot\mathbf{r}}, \quad u_{n\mathbf{k}+\mathbf{g}} = \begin{bmatrix} f_{n\mathbf{k}+\mathbf{g}} \\ \psi_{n1\mathbf{k}+\mathbf{g}} \\ \psi_{n2\mathbf{k}+\mathbf{g}} \\ \vdots \end{bmatrix}, \tag{35}$$

where $\tilde{u}_{n\mathbf{k}}(\mathbf{r}+\mathbf{R}) = \tilde{u}_{n\mathbf{k}}(\mathbf{r})$ is periodic in the atomic crystal lattice and we have normalized by the unit cell area V. In this basis, $\tilde{u}_{n\mathbf{k}}(\mathbf{r})$ is normalized to unit energy as

$$1 = \int_{\text{cell}} d^2\mathbf{r}\, \tilde{u}_{n\mathbf{k}}^{\dagger}(\mathbf{r}) \tilde{u}_{n\mathbf{k}}(\mathbf{r}) = \sum_{\mathbf{g}} u_{n\mathbf{k}+\mathbf{g}}^{\dagger} u_{n\mathbf{k}+\mathbf{g}} = \sum_{\mathbf{g}} \left(f_{n\mathbf{k}+\mathbf{g}}^{\dagger} f_{n\mathbf{k}+\mathbf{g}} + \sum_{\alpha} \psi_{n\alpha\mathbf{k}+\mathbf{g}}^{\dagger} \psi_{n\alpha\mathbf{k}+\mathbf{g}} \right) = \sum_{\mathbf{g}\mathbf{g}'} f_{n\mathbf{k}+\mathbf{g}}^{\dagger} \bar{\mathcal{M}}_{\mathbf{g}'-\mathbf{g}}(\omega_{n\mathbf{k}}, \mathbf{k}+\mathbf{g}) f_{n\mathbf{k}+\mathbf{g}'}. \tag{36}$$

The integration is taken over the 2D unit cell. To simplify Eq. (36), we have utilized the linear response theory to express ψ_{α} in terms of the driving field f,

$$\psi_{n\alpha\mathbf{k}+\mathbf{g}} = \frac{\sum_{\mathbf{g}'} \mathcal{C}_{\alpha\mathbf{g}'}(\mathbf{k}+\mathbf{g}) f_{n\mathbf{k}+\mathbf{g}'+\mathbf{g}}}{\omega_{n\mathbf{k}} - \omega_{\alpha\mathbf{k}+\mathbf{g}}}. \tag{37}$$

$\bar{\mathcal{M}}_{\mathbf{g}}(\omega,\mathbf{k}) = \partial_{\omega}[\omega \mathcal{M}_{\mathbf{g}}(\omega,\mathbf{k})]$ is the contribution to the energy density arising from each spatial harmonic of the crystal.

Finally, the eigenenergies $\omega_{n\mathbf{k}}$ are the n nontrivial roots of the characteristic wave equation,

$$\mathcal{H}_0(\mathbf{k}) f_{n\mathbf{k}} = \omega_{n\mathbf{k}} \sum_{\mathbf{g}} \mathcal{M}_{\mathbf{g}}(\omega_{n\mathbf{k}}, \mathbf{k}) f_{n\mathbf{k}+\mathbf{g}}, \tag{38}$$

which generates all possible photonic bands of the crystal. Note, the response function $\mathcal{M}_{\mathbf{g}}(\omega,\mathbf{k})$ is now expressed in terms of $\mathcal{C}_{\alpha\mathbf{g}}(\mathbf{k})$ and describes the net summation of all scattering and backscattering events in the material,

$$\mathcal{M}_{\mathbf{g}}(\omega,\mathbf{k}) = \mathbb{1}_3 \delta_{\mathbf{g}} - \sum_{\alpha\mathbf{g}'} \frac{\mathcal{C}_{\alpha-\mathbf{g}'}^{\dagger}(\mathbf{k}+\mathbf{g}') \mathcal{C}_{\alpha\mathbf{g}-\mathbf{g}'}(\mathbf{k}+\mathbf{g}')}{\omega_{\alpha\mathbf{k}+\mathbf{g}'}(\omega - \omega_{\alpha\mathbf{k}+\mathbf{g}'})}. \tag{39}$$

This proves that the wave equation is derived from a first-order Hamiltonian, has real eigenvalues $\omega = \omega_{n\mathbf{k}}$ for all momenta, and is normalizable with respect to the total state vector $\tilde{u}_{n\mathbf{k}}(\mathbf{r})$.

III. DISCRETE ROTATIONAL SYMMETRY

A. Point groups in 2D

Point groups are the discrete analogs of continuous rotations and reflections. They represent the number of ways the atomic lattice can be transformed into itself [95,96]. Due to the crystallographic restriction theorem, there are ten such point groups in 2D. The first five are the cyclic groups C_N,

$$C_1,\ C_2,\ C_3,\ C_4,\ C_6. \tag{40}$$

For instance, C_3 implies threefold cyclic symmetry while C_1 is no symmetry. The last five are the dihedral groups D_N,

$$D_1,\ D_2,\ D_3,\ D_4,\ D_6. \tag{41}$$

The dihedral group D_N contains C_N plus reflections. However, it can be proven that the Chern number for all D_N point groups vanish [72]. In fact, any space group containing mirror symmetry has a vanishing Chern number [73]. Therefore, we concern ourselves with only the (Abelian) cyclic groups C_N. The Brillouin zone of each point group is displayed in Fig. 1.

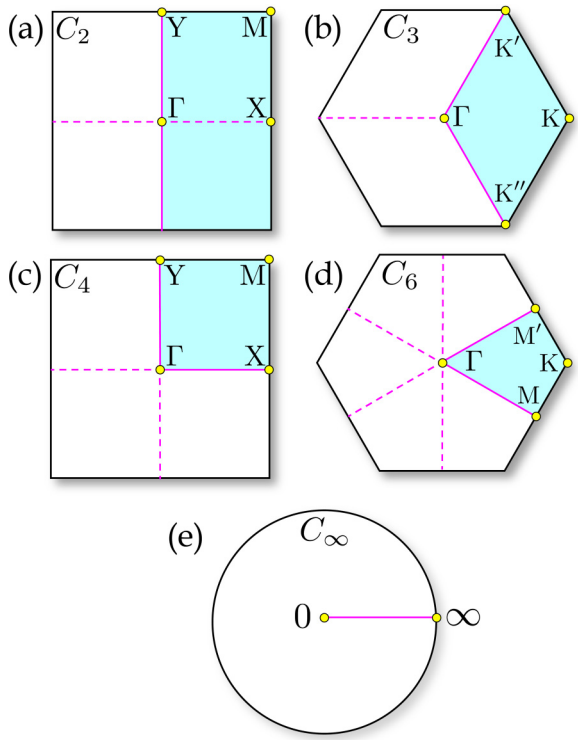

FIG. 1. Brillouin zone of each cyclic point group C_N. (a), (b), (c), (d), and (e) correspond to $N = 2,\ 3,\ 4,\ 6$, and ∞, respectively. Due to rotational symmetry, the total Brillouin zone is equivalent to N copies of the irreducible Brillouin zone (IBZ), which is represented by the blue quadrant. For continuous symmetry $N = \infty$, this is simply a line. The yellow circles label high-symmetry points $R\mathbf{k}_i = \mathbf{k}_i$ where the crystal Hamiltonian is invariant under a certain rotation $\hat{\mathcal{R}}$. At these specific momenta, a Bloch photonic wave function $\mathcal{R}\tilde{f}_{\mathbf{k}_i}(R^{-1}\mathbf{r}) = \eta(\mathbf{k}_i)\tilde{f}_{\mathbf{k}_i}(\mathbf{r})$ is an eigenstate of an N-fold rotation $\eta(\mathbf{k}_i) = \eta_N(\mathbf{k}_i) = [i\frac{2\pi}{N}m_N(\mathbf{k}_i)]$ such that the photon possesses quantized integer eigenvalues $m_N(\mathbf{k}_i) \in \mathbb{Z}_N$. Since m_N are discrete quantum numbers, their values cannot vary continuously if the crystal symmetry is preserved; they can only be changed at a topological phase transition.

The defining characteristic of each cyclic group is the fermionic or bosonic representation. When we rotate the fields by 2π, we take the particle into itself and acquire a phase,

$$\mathcal{R}(2\pi) = (-1)^F. \tag{42}$$

F is twice the total spin of the particle, or equivalently, the fermion number. Fermions with half-integer spin are anti-symmetric under rotations $\mathcal{R}(2\pi) = -1$, while bosons with integer spin are symmetric $\mathcal{R}(2\pi) = +1$. Depending on the symmetries of the lattice, the topology fundamentally changes for fermions and bosons. We will understand the implications this has for spin-1 photons.

B. Spin-1 discrete symmetries

If the two-dimensional crystal belongs to a cyclic point group C_N, the Hamiltonian possesses discrete rotational symmetry about the z axis,

$$\mathcal{R}^{-1}H_{R\mathbf{g}}(R\mathbf{k})\mathcal{R} = H_{\mathbf{g}}(\mathbf{k}), \quad \omega_{nR\mathbf{k}} = \omega_{n\mathbf{k}}, \tag{43}$$

where $\mathcal{R}$ is any rotation in C_N. The eigenenergies $\omega_{n\mathbf{k}}$ respect the symmetry of the crystal; the energy at $R\mathbf{k}$ and $\mathbf{k}$ is identical. It is important to note that $\mathcal{R}$ is *diagonal* in u, meaning the photon and each oscillator is rotated individually, $f \to \mathcal{R}f$ and $\psi_\alpha \to \mathcal{R}\psi_\alpha$. This implies there is no mixing of fields. The symmetries of the Hamiltonian are endowed by the coupling tensors, which dictates the degrees of freedom of the material response,

$$\mathcal{R}^{-1}\mathcal{C}_{\alpha R\mathbf{g}}(R\mathbf{k})\mathcal{R} = \mathcal{C}_{\alpha\mathbf{g}}(\mathbf{k}), \quad \omega_{\alpha R\mathbf{k}} = \omega_{\alpha\mathbf{k}}. \tag{44}$$

After summation over all $\mathcal{C}_{\alpha\mathbf{g}}(\mathbf{k})$, we can prove that the response function transforms identically under such a rotation,

$$\mathcal{R}^{-1}\mathcal{M}_{R\mathbf{g}}(\omega, R\mathbf{k})\mathcal{R} = \mathcal{M}_{\mathbf{g}}(\omega, \mathbf{k}). \tag{45}$$

Therefore, the photon inherits all symmetries of the crystal.

In this case, the $\mathcal{R}$ matrix represents a discrete rotation and can be expressed as the exponential of the spin-1 generator $(\hat{S}_z)_{ij} = -i\epsilon_{ijz}$,

$$\mathcal{R}_N = \exp\left(-i\frac{2\pi}{N}\hat{S}_z\right) = \begin{bmatrix} R_N & 0 \\ 0 & 1 \end{bmatrix}, \tag{46}$$

where $\frac{2\pi}{N}$ is an N-fold rotation,

$$R_N = \begin{bmatrix} \cos\left(\frac{2\pi}{N}\right) & -\sin\left(\frac{2\pi}{N}\right) \\ \sin\left(\frac{2\pi}{N}\right) & \cos\left(\frac{2\pi}{N}\right) \end{bmatrix}. \tag{47}$$

Electric components transform as 2D vectors and rotate into one another under $\mathcal{R}$. Magnetic components transform as scalars and are left invariant under $\mathcal{R}$. We stress that every cyclic group for the photon is a vector representation, which is *bosonic*,

$$(\mathcal{R}_N)^N = \mathcal{R}(2\pi) = +\mathbb{1}_3. \tag{48}$$

The electromagnetic field returns in phase under cyclic revolution.

C. High-symmetry points

The Bloch eigenstates $\tilde{u}_{n\mathbf{k}}(\mathbf{r})$ are essentially a collection of periodic vector fields. To rotate the fields, we must perform an operation on both the coordinates $\mathbf{r}$ and the polarization states f and ψ_α. In real space, the operation of a rotation $\hat{\mathcal{R}}$ is performed as

$$\mathcal{R}\tilde{u}_{n\mathbf{k}}(R^{-1}\mathbf{r}) = \eta_n(\mathbf{k})\tilde{u}_{nR\mathbf{k}}(\mathbf{r}), \tag{49}$$

where $\mathcal{R}$ is a discrete rotation defined in Eq. (46). This implies the Fourier coefficients obey,

$$\mathcal{R}u_{n\mathbf{k}+R^{-1}\mathbf{g}} = \eta_n(\mathbf{k})u_{nR\mathbf{k}+\mathbf{g}}. \tag{50}$$

It follows from symmetry that the operation of $\hat{\mathcal{R}}$ takes a wave function at $\mathbf{k}$ to $R\mathbf{k}$ with the same energy $\omega_{n\mathbf{k}} = \omega_{nR\mathbf{k}}$, but with a possibly different phase $|\eta_n(\mathbf{k})|^2 = 1$. Utilizing the linear response theory, we notice that the phase factor $\eta_n(\mathbf{k})$ is governed entirely by the photon,

$$\mathcal{R}\psi_{n\alpha\mathbf{k}+R^{-1}\mathbf{g}} = \frac{\sum_{\mathbf{g}'}\mathcal{R}\mathcal{C}_{\alpha\mathbf{g}'}(\mathbf{k}+R^{-1}\mathbf{g})f_{n\mathbf{k}+\mathbf{g}'+R^{-1}\mathbf{g}}}{\omega_{n\mathbf{k}} - \omega_{\alpha\mathbf{k}+R^{-1}\mathbf{g}}}$$

$$= \frac{\sum_{\mathbf{g}'}\mathcal{C}_{\alpha R\mathbf{g}'}(R\mathbf{k}+\mathbf{g})\mathcal{R}f_{n\mathbf{k}+\mathbf{g}'+R^{-1}\mathbf{g}}}{\omega_{n\mathbf{k}} - \omega_{\alpha\mathbf{k}+R^{-1}\mathbf{g}}}$$

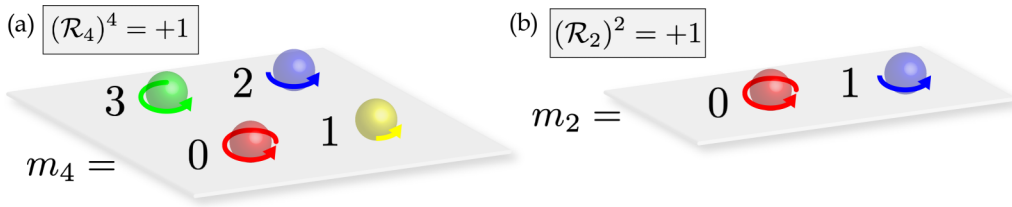

FIG. 2. The collection of spin-1 (bosonic) charges for the C_4 point group. (a) Fourfold rotations $(\mathcal{R}_4)^4 = +1$; there are four unique eigenvalues $\eta_4 = \exp[i\frac{2\pi}{4}m_4]$ corresponding to the roots of unity $(\eta_4)^4 = +1$. These represent the modulo 4 integers $m_4 \in \mathbb{Z}_4$. Note that $m_4 = 3 = -1$ can also be interpreted as a left-handed eigenstate. (b) Bosonic inversion $(\mathcal{R}_2)^2 = +1$; there are two unique eigenvalues $\eta_2 = \exp[i\frac{2\pi}{2}m_2]$ corresponding to the roots of unity $(\eta_2)^2 = +1$. These represent the modulo 2 integers $m_2 \in \mathbb{Z}_2$.

$$= \frac{\sum_{\mathbf{g}'} \mathcal{C}_{\alpha\mathbf{g}'}(R\mathbf{k}+\mathbf{g})\eta_n(\mathbf{k}) f_{nR\mathbf{k}+\mathbf{g}'+\mathbf{g}}}{\omega_{n\mathbf{k}} - \omega_{\alpha R\mathbf{k}+\mathbf{g}}}$$

$$= \eta_n(\mathbf{k})\psi_{n\alpha R\mathbf{k}+\mathbf{g}}. \tag{51}$$

This is an incredibly convenient simplification and implies the precise coordinates of the matter oscillations ψ_α are superfluous when discussing symmetries. The electromagnetic field f tells us everything.

Importantly, there are specific points in the Brillouin zone where $\mathbf{k}$ is invariant under a discrete rotation,

$$R\mathbf{k}_i = \mathbf{k}_i. \tag{52}$$

This is because the crystal momentum only differs by a lattice translation at these points $R\mathbf{k}_i = \mathbf{k}_i + \mathbf{g}$, which leaves a Bloch wave function unchanged,

$$e^{iR\mathbf{k}_i\cdot\mathbf{r}}\tilde{u}_{nR\mathbf{k}_i}(\mathbf{r}) = e^{i(\mathbf{k}_i+\mathbf{g})\cdot\mathbf{r}}\tilde{u}_{n\mathbf{k}_i+\mathbf{g}}(\mathbf{r})$$
$$= e^{i\mathbf{k}_i\cdot\mathbf{r}}\tilde{u}_{n\mathbf{k}_i}(\mathbf{r}). \tag{53}$$

These are called *high-symmetry points* (HSPs); they occur at the center and certain vertices of the Brillouin zone. The crystal Hamiltonian is *rotationally invariant* at these momenta, i.e., it commutes with $\hat{\mathcal{R}}$. Therefore, the wave functions are simultaneous eigenstates of $\hat{\mathcal{R}}$ at HSPs,

$$\mathcal{R}\tilde{u}_{n\mathbf{k}_i}(R^{-1}\mathbf{r}) = \eta_n(\mathbf{k}_i)\tilde{u}_{n\mathbf{k}_i}(\mathbf{r}), \tag{54}$$

which immediately implies

$$\mathcal{R}\tilde{f}_{n\mathbf{k}_i}(R^{-1}\mathbf{r}) = \eta_n(\mathbf{k}_i)\tilde{f}_{n\mathbf{k}_i}(\mathbf{r}). \tag{55}$$

Here, $\eta_n(\mathbf{k}_i)$ is the eigenvalue of $\hat{\mathcal{R}}$ at $\mathbf{k}_i$ for the nth band.

D. Spin-1 eigenvalues

Depending on the point group and the precise HSP, $\eta_n(\mathbf{k}_i) = \eta_{N,n}(\mathbf{k}_i)$ can represent any Nth root of unity corresponding to the N-fold rotation operator $\hat{\mathcal{R}}_N$,

$$\eta_{N,n}(\mathbf{k}_i) = \exp\left[i\frac{2\pi}{N}m_{N,n}(\mathbf{k}_i)\right], \quad (\eta_{N,n})^N = +1. \tag{56}$$

$m_{N,n}(\mathbf{k}_i) \in \mathbb{Z}_N$ is a modulo integer; it labels the N possible spin-1 eigenvalues at $\mathbf{k}_i$. In C_4, for example, the Γ and M points are invariant under $\hat{\mathcal{R}}_4$ rotations, while the X and Y points are invariant under $\hat{\mathcal{R}}_2$ rotations (inversion). This means there are four possible spin-1 charges located at $m_{4,n}(\Gamma)$ and $m_{4,n}(M) \in \mathbb{Z}_4$, respectively, and two possible charges located at $m_{2,n}(X) = m_{2,n}(Y) \in \mathbb{Z}_2$. A visualization of these topological charges is presented in Fig. 2 and this is contrasted with their fermionic counterparts in Fig. 3. In Sec. IV we will connect these rotational eigenvalues directly to the topological invariants.

IV. TOPOLOGICAL ELECTROMAGNETIC (BOSONIC) PHASES OF MATTER

A. Electromagnetic Chern number

The Berry connection for a band n is found by varying the total Bloch wave function $\tilde{u}_{n\mathbf{k}}(\mathbf{r})$ with respect to the momentum,

$$\mathbf{A}_n(\mathbf{k}) = -i\int_{\text{cell}} d^2\mathbf{r}\, \tilde{u}^\dagger_{n\mathbf{k}}(\mathbf{r})\partial_{\mathbf{k}}\tilde{u}_{n\mathbf{k}}(\mathbf{r})$$
$$= -i\sum_{\mathbf{g}} u^\dagger_{n\mathbf{k}+\mathbf{g}}\partial_{\mathbf{k}}u_{n\mathbf{k}+\mathbf{g}}. \tag{57}$$

This can be simplified slightly to obtain

$$\mathbf{A}_n(\mathbf{k}) = -i\sum_{\mathbf{g}\mathbf{g}'} f^\dagger_{n\mathbf{k}+\mathbf{g}}\bar{\mathcal{M}}_{\mathbf{g}'-\mathbf{g}}(\omega_{n\mathbf{k}}, \mathbf{k}+\mathbf{g})\partial_{\mathbf{k}}f_{n\mathbf{k}+\mathbf{g}'}$$
$$+\sum_{\mathbf{g}\mathbf{g}'} f^\dagger_{n\mathbf{k}+\mathbf{g}}\boldsymbol{\mathcal{A}}_{\mathbf{g}'-\mathbf{g}}(\omega_{n\mathbf{k}}, \mathbf{k}+\mathbf{g})f_{n\mathbf{k}+\mathbf{g}'}. \tag{58}$$

The first term gives the Berry connection of the photon, while the second term $\boldsymbol{\mathcal{A}}_{\mathbf{g}}(\omega, \mathbf{k})$ arises solely from the matter oscillations,

$$\boldsymbol{\mathcal{A}}_{\mathbf{g}}(\omega, \mathbf{k}) = -i\sum_{\alpha\mathbf{g}'}\frac{\mathcal{C}^\dagger_{\alpha-\mathbf{g}'}(\mathbf{k}+\mathbf{g}')\partial_{\mathbf{k}}\mathcal{C}_{\alpha\mathbf{g}-\mathbf{g}'}(\mathbf{k}+\mathbf{g}')}{(\omega-\omega_{\alpha\mathbf{k}+\mathbf{g}'})^2}. \tag{59}$$

Due to nonlocality, Eq. (59) does not generally vanish. This additional contribution to the Berry phase corresponds to vortices in the response function itself, independent of the Berry gauge of the photon. This means the Chern number can be nonzero $\mathfrak{C}_n \neq 0$ even if the winding of electromagnetic field is trivial. However, we will show in the proceeding sections that all symmetry constraints on the Chern number can be established entirely in terms of the photon.

As can be seen from Eq. (58), the Berry connection is only defined within the Brillouin zone $\mathbf{A}_{n\mathbf{k}+\mathbf{g}} = \mathbf{A}_{n\mathbf{k}} + \partial_{\mathbf{k}}\chi_{n\mathbf{k}}$, up to a possible U(1) gauge. Hence, the gauge invariant Berry curvature is periodic $F_{n\mathbf{k}+\mathbf{g}} = F_{n\mathbf{k}}$,

$$F_n(\mathbf{k}) = \hat{\mathbf{z}}\cdot[\partial_{\mathbf{k}}\times\mathbf{A}_n(\mathbf{k})]. \tag{60}$$

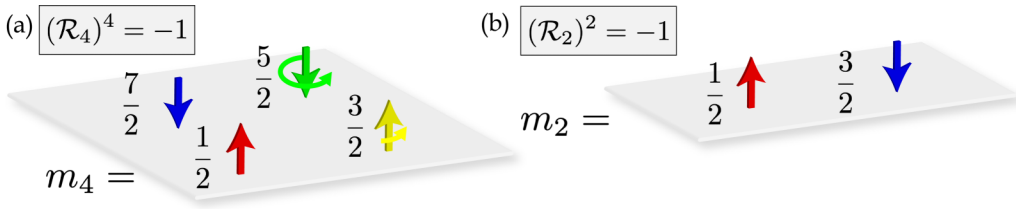

FIG. 3. The collection of spin-$\frac{1}{2}$ (fermionic) charges for the C_4 point group. (a) Fourfold rotations $(\mathcal{R}_4)^4 = -1$; there are four unique eigenvalues $\zeta_4 = \exp[i\frac{2\pi}{4}m_4]$ corresponding to the roots of negative unity $(\zeta_4)^4 = -1$. These represent the modulo 4 half-integers $m_4 \in \mathbb{Z}_4 + \frac{1}{2}$. Note that $m_4 = \frac{7}{2} = -\frac{1}{2}$ can be interpreted as a spin-down fermion while $m_4 = \frac{3}{2} = \frac{1}{2} + 1$ and $m_4 = \frac{5}{2} = -\frac{1}{2} + 3$ constitute a fermion plus a boson. (b) Fermionic inversion $(\mathcal{R}_2)^2 = -1$; there are two unique eigenvalues $\zeta_2 = \exp[i\frac{2\pi}{2}m_2]$ corresponding to the roots of negative unity $(\zeta_2)^2 = -1$. These represent the modulo 2 half-integers $m_2 \in \mathbb{Z}_2 + \frac{1}{2}$. Note that $m_2 = \frac{3}{2} = -\frac{1}{2}$ can also be interpreted as a spin-down fermion under modulo 2.

The Chern number is found by integrating the Berry curvature over the two-dimensional Brillouin zone,

$$\mathfrak{C}_n = \frac{1}{2\pi}\int_{\mathrm{BZ}} F_n(\mathbf{k})d^2\mathbf{k}, \quad \mathfrak{C}_n \in \mathbb{Z}, \tag{61}$$

which determines the winding number of the collective light-matter excitations over the torus $\mathbb{T}^2 = S^1 \times S^1$. Equation (61) is one of the central results of this paper. An electromagnetic Chern invariant can be found for any 2D crystal and characterizes distinct topological phases of matter $\mathfrak{C}_n \neq 0$.

B. Symmetry-protected topological bosonic phases

Evaluating the Chern number by brute force requires knowledge of the wave function at every point in the Brillouin zone. However, by invoking symmetry constraints of the cyclic groups, we can determine important properties of the topological phase from only a few isolated points in the Brillouin zone. This constitutes a type of SPT phase [69–80] and is intimately tied to the spin-1 nature of electromagnetic field. SPT phases are protected by the N-fold rotational symmetry of C_N and this gives rise to an additional topological invariant $\nu_n \in \mathbb{Z}_N$. Remarkably, ν_n is classified entirely from $\eta_n(\mathbf{k}_i)$ eigenvalues at HSPs and requires no complicated integration to compute. This invariant is related to the Chern number up to a multiple of N,

$$\nu_n = \mathfrak{C}_n \mod N, \quad \mathfrak{C}_n \in N\mathbb{Z} + \nu_n. \tag{62}$$

The interpretation of ν_n is quite simple; it tells us the geometric phase around the irreducible Brillouin zone (IBZ) of the crystal,

$$\exp\left(i\frac{2\pi}{N}\mathfrak{C}_n\right) = \exp\left(i\int_{\mathrm{IBZ}} F_n(\mathbf{k})d^2\mathbf{k}\right) = \exp\left(i\oint_{\partial\mathrm{IBZ}} \mathbf{A}_n(\mathbf{k})\cdot d\mathbf{k}\right), \tag{63}$$

where ∂IBZ is the path around IBZ. This follows from rotational symmetry of the Berry curvature $F_n(\mathbf{k}) = F_n(R\mathbf{k})$. For instance, the path in C_4 is $\partial(\mathrm{IBZ})_4 = \Gamma XMY\Gamma$. Applying the logarithm, ν_n is equivalent to

$$\nu_n = \frac{N}{2\pi}\oint_{\partial\mathrm{IBZ}} \mathbf{A}_n(\mathbf{k})\cdot d\mathbf{k} \mod N. \tag{64}$$

As we will see more explicitly, ν_n is tied entirely to η_n. The reason is subtle; any vortex within the interior of the IBZ contributes a Berry phase of 2π, and by symmetry, there are N such vortices within the total Brillouin zone $\mathfrak{C}_n \to \mathfrak{C}_n + N$. However, this has no effect on $\nu_n \to \nu_n$. Only the vortices lying at HSPs contribute to ν_n because these come in fractions of 2π.

In the following sections we will discuss the bosonic classification of ν_n for each cyclic point group and the SPT phases associated with them. We do not present the full derivations here since the rigorous proofs have been carried out by others (see Ref. [72]), we simply state the salient results. For completeness, in Appendix A we also discuss the SPT *fermionic* phases associated with each point group. We do this to emphasize that fermionic and bosonic systems represent distinct topological field theories, with fundamentally different interpretations. These differences are highlighted with a few examples (Figs. 4 and 5).

C. Twofold (inversion) symmetry: C_2

For the C_2 point group, or simply inversion symmetry, the SPT phase is related to the Chern number by $\nu_n = \mathfrak{C}_n \mod 2$ which is a $\mathbb{Z}_2$ invariant. There is only one nontrivial SPT phase and it can be found modulo 2 from

$$\exp\left(i\frac{2\pi}{2}\mathfrak{C}_n\right) = \eta_{2,n}(\Gamma)\eta_{2,n}(X)\eta_{2,n}(Y)\eta_{2,n}(M). \tag{65}$$

Applying the logarithm, this classification can be expressed equivalently in terms of $m_{2,n} \in \mathbb{Z}_2$ inversion eigenvalues,

$$\nu_n = m_{2,n}(\Gamma) + m_{2,n}(X) + m_{2,n}(Y) + m_{2,n}(M) \mod 2. \tag{66}$$

If the summation of $m_{2,n}$ eigenvalues is odd, the SPT phase is nontrivial $\nu_n = 1$ and corresponds to an odd-valued Chern number. Likewise, $\nu_n = 0$ is an even-valued Chern number.

D. Threefold symmetry: C_3

C_3 is unique because it is the only point group with an odd rotational symmetry; i.e., it lacks inversion symmetry. This means the parity of the Chern number (odd or even) is not restricted by the symmetries of the crystal. For C_3, the SPT phase is $\nu_n = \mathfrak{C}_n \mod 3$, which is a $\mathbb{Z}_3$ invariant. There are two nontrivial SPT phases and they can be found modulo 3 from

$$\exp\left(i\frac{2\pi}{3}\mathfrak{C}_n\right) = \eta_{3,n}(\Gamma)\eta_{3,n}(K)\eta_{3,n}(K'). \tag{67}$$

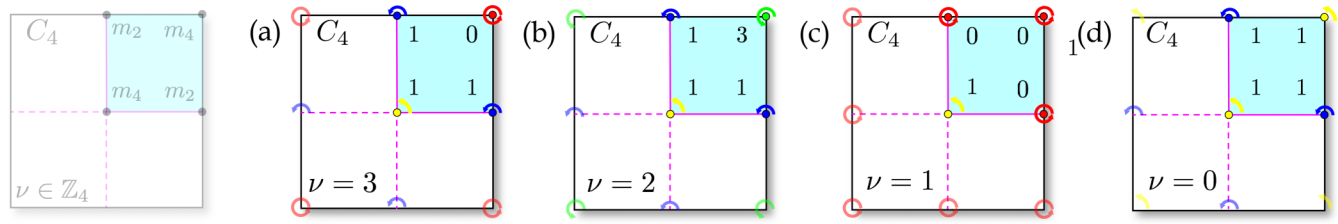

FIG. 4. Examples of SPT bosonic phases in a crystal with C_4 symmetry. These phases are characterized by their SPT invariant $\nu = m_4(\Gamma) + m_4(M) + 2m_2(Y) \mod 4$, which determines the electromagnetic Chern number up to a multiple of 4. Here, $m_4 \in \mathbb{Z}_4$ and $m_2 \in \mathbb{Z}_2$ are modulo integers. (a), (b), (c), and (d) correspond to SPT bosonic phases of $\nu = 3,\ 2,\ 1$, and 0, respectively. For bosons, we simply add up all the integer charges within the irreducible Brillouin zone. For instance, the $\nu = 2$ phase has eigenvalues of $m_4(\Gamma) = 1$ at the center and $m_4(M) = 3 = -1$ at the vertices, with inversion eigenvalues of $m_2(Y) = m_2(X) = 1$ at the edge centers: $\nu = 1 + 3 + 2 \times 1 = 2$.

This classification is expressed equivalently in terms of quantized modulo 3 integers $m_{3,n} \in \mathbb{Z}_3$ at HSPs,

$$\nu_n = m_{3,n}(\Gamma) + m_{3,n}(K) + m_{3,n}(K') \mod 3. \tag{68}$$

Note though, odd and even phases are not distinct $\nu = -2 = 1 = 4$ under modulo 3.

E. Fourfold symmetry: C_4

For the C_4 point group, the SPT phase is related to the Chern number by $\nu_n = \mathfrak{C}_n \mod 4$, which is a $\mathbb{Z}_4$ invariant. There are three nontrivial SPT phases and they can be found modulo 4 from

$$\exp\left(i\frac{2\pi}{4}\mathfrak{C}_n\right) = \eta_{4,n}(\Gamma)\eta_{4,n}(M)\eta_{2,n}(Y). \tag{69}$$

The classification is expressed equivalently in terms of spin-1 eigenvalues,

$$\nu_n = m_{4,n}(\Gamma) + m_{4,n}(M) + 2m_{2,n}(Y) \mod 4, \tag{70}$$

where $m_{4,n}(\Gamma)$ and $m_{4,n}(M) \in \mathbb{Z}_4$ are modulo 4 integers and $m_{2,n}(Y) \in \mathbb{Z}_2$ is a modulo 2 integer. Examples of all SPT phases of the C_4 point group are displayed in Fig. 4 and these are compared with their fermionic counterparts in Fig. 5.

F. Sixfold symmetry: C_6

For the C_6 point group, the SPT phase is $\nu_n = \mathfrak{C}_n \mod 6$, which is a $\mathbb{Z}_6$ invariant. There are five nontrivial SPT phases and they can be found modulo 6 from

$$\exp\left(i\frac{2\pi}{6}\mathfrak{C}_n\right) = \eta_{6,n}(\Gamma)\eta_{3,n}(K)\eta_{2,n}(M). \tag{71}$$

This is equivalent to the summation of spin-1 eigenvalues at the HSPs,

$$\nu_n = m_{6,n}(\Gamma) + 2m_{3,n}(K) + 3m_{2,n}(M) \mod 6, \tag{72}$$

where $m_{6,n}(\Gamma) \in \mathbb{Z}_6$ is a modulo 4 integer, $m_{3,n}(K) \in \mathbb{Z}_3$ is a modulo 3 integer, and $m_{2,n}(M) \in \mathbb{Z}_2$ is a modulo 2 integer. This completes the classification of all 2+1D topological electromagnetic (bosonic) phases of matter which is summarized in Table I. These are compared alongside their fermionic counterparts in Table II.

G. Continuous symmetry: C_∞

To finish, we briefly discuss the continuum limit $\mathbf{g} = \mathbf{0}$ and the topological phases that can be described by a long-wavelength theory $k \approx 0$. The physics is significantly more tractable here and exactly solvable models are possible [25–27]. In this limit, the rotational symmetry of the crystal is approximately continuous C_∞. The SPT invariant ν_n and Chern number $\mathfrak{C}_n$ are thus equivalent,

$$\nu_n = \mathfrak{C}_n = m_n(0) - m_n(\infty). \tag{73}$$

Note that $\nu_n \in \mathbb{Z}$ and $m_n \in \mathbb{Z}$ are *not* modulo integers in this limit and do not have the same interpretation as the lattice theory. This is because we have gained the full rotational symmetry in the continuum approximation. Note that for

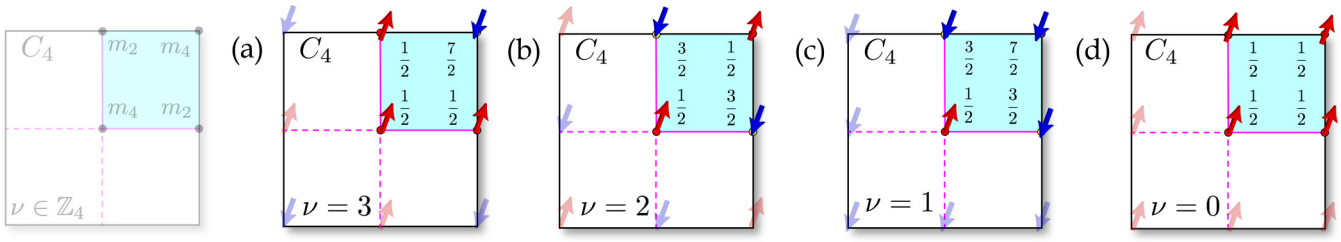

FIG. 5. Examples of SPT fermionic phases in a crystal with C_4 symmetry. These phases are characterized by their SPT invariant $\nu = m_4(\Gamma) + m_4(M) + 2m_2(Y) + 2 \mod 4$, which determines the electronic Chern number up to a multiple of 4. In this case, $m_4 \in \mathbb{Z}_4 + \frac{1}{2}$ and $m_2 \in \mathbb{Z}_2 + \frac{1}{2}$ are modulo *half*-integers. (a), (b), (c), and (d) correspond to SPT fermionic phases of $\nu = 3,\ 2,\ 1$, and 0, respectively. The problem is more complicated for fermions because the charges are fractional and we must also account for the antisymmetric phases of a spinor wave function. As an example, the $\nu = 2$ phase has eigenvalues of $m_4(\Gamma) = m_4(M) = \frac{1}{2}$ at the center and vertices, with inversion eigenvalues of $m_2(Y) = m_2(X) = \frac{3}{2} = -\frac{1}{2}$ at the edge centers: $\nu = \frac{1}{2} + \frac{1}{2} + 2 \times \frac{3}{2} + 2 = 2$.

fermions, $m_n \in \mathbb{Z} + \frac{1}{2}$ is a half-integer. Clearly though, the spin eigenvalues must change at HSPs $m_n(0) \neq m_n(\infty)$ for a nontrivial phase to exist $\mathfrak{C}_n \neq 0$. In the continuum regularization, $k_i = 0$ represents the Γ point and $k_i = \infty$ is interpreted as mapping the vertices of the Brillouin zone into one another. We have provided a simple example of a continuum topological electromagnetic phase in Appendix B.

V. CONCLUSIONS

In summary, we have developed the complete 2+1D lattice field theory describing symmetry-protected topological bosonic phases of the photon. To accomplish this, we analyzed the electromagnetic Bloch waves in microscopic crystals and derived the Chern invariant of these light-matter excitations. Thereafter, the rotational symmetries of the crystal were examined extensively and the implications these have on photonic spin. We have studied all two-dimensional point groups C_N with nonvanishing Chern number $\mathfrak{C} \neq 0$ and linked the topological invariants directly to spin-1 quantized eigenvalues of the electromagnetic field, establishing the bosonic classification for each topological phase.

ACKNOWLEDGMENTS

This research was supported by the Defense Advanced Research Projects Agency (DARPA) Nascent Light-Matter Interactions (NLM) Program and the National Science Foundation (NSF) (Grant No. EFMA-1641101).

APPENDIX A: SYMMETRY-PROTECTED TOPOLOGICAL FERMIONIC PHASES

For completeness, we examine the SPT fermionic phases associated with each point group C_N and highlight their essential differences from bosons. The most important distinction is how they transform under rotations; half-integer particles are antisymmetric $\mathcal{R}(2\pi) = -1$. In terms of discrete rotations $\hat{\mathcal{R}}_N$ about the z axis, the eigenstates of a Bloch spinor particle satisfy

$$\hat{\mathcal{R}}_N|\Psi_{\mathbf{k}_i}\rangle = \zeta_N(\mathbf{k}_i)|\Psi_{\mathbf{k}_i}\rangle, \tag{A1}$$

where the eigenvalues at HSPs are related by

$$\zeta_N(\mathbf{k}_i) = \exp\left[i\frac{2\pi}{N}m_N(\mathbf{k}_i)\right], \quad (\zeta_N)^N = -1. \tag{A2}$$

$m_N(\mathbf{k}_i) \in \mathbb{Z}_N + \frac{1}{2}$ is a modulo half-integer and labels the N possible spin-$\frac{1}{2}$ eigenvalues. Notice that ζ_N represents the Nth roots of *negative* unity which is characteristic of a fermionic field.

The single-particle fermionic classification for C_2, C_3, C_4, and C_6, respectively, is [72,79]

$$\exp\left(i\frac{2\pi}{2}\mathfrak{C}\right) = \zeta_2(\Gamma)\zeta_2(X)\zeta_2(Y)\zeta_2(M), \tag{A3a}$$

$$\exp\left(i\frac{2\pi}{3}\mathfrak{C}\right) = -\zeta_3(\Gamma)\zeta_3(K)\zeta_3(K'), \tag{A3b}$$

$$\exp\left(i\frac{2\pi}{4}\mathfrak{C}\right) = -\zeta_4(\Gamma)\zeta_4(M)\zeta_2(Y), \tag{A3c}$$

$$\exp\left(i\frac{2\pi}{6}\mathfrak{C}\right) = -\zeta_6(\Gamma)\zeta_3(K)\zeta_2(M). \tag{A3d}$$

Although the classification appears similar, the SPT fermionic phases constitute very different physics than their bosonic counterparts, which is alluded to by the antisymmetric phase factors $\mathcal{R}(2\pi) = -1$. We illustrate this with an example in C_4. Applying the logarithm, the classification for the SPT fermionic phase $\nu = \mathfrak{C} \mod 4$ can be expressed as

$$\nu = m_4(\Gamma) + m_4(M) + 2m_2(Y) + 2 \mod 4, \tag{A4}$$

where $m_4(\Gamma)$ and $m_4(M) \in \mathbb{Z}_4 + \frac{1}{2}$ are modulo 4 half-integers and $m_2(Y) \in \mathbb{Z}_2 + \frac{1}{2}$ is a modulo 2 half-integer.

APPENDIX B: EXAMPLE OF A CONTINUUM TOPOLOGICAL ELECTROMAGNETIC PHASE

We consider the long-wavelength (continuum) limit $k \approx 0$ and ignore all higher order $\mathbf{g} \neq \mathbf{0}$ spatial harmonics [25–27]. The simplest response function showing a topologically nontrivial electromagnetic phase is described by the permittivity tensor ε_{ij},

$$\varepsilon_{ij}(\omega, k) = \varepsilon(\omega, k)\delta_{ij} + ig(\omega, k)\epsilon_{ij}. \tag{B1}$$

$\epsilon_{ij} = -\epsilon_{ji}$ is the antisymmetric tensor and should not be confused with the permittivity ε_{ij}. This is simply the Drude model biased under an applied magnetic field. ε is the scalar permittivity (diagonal part),

$$\varepsilon(\omega, k) = 1 + \frac{\omega_p^2(k)}{\omega_c^2(k) - \omega^2}, \tag{B2}$$

while g is the gyrotropic coefficient (off-diagonal part) which breaks both parity and time-reversal symmetry,

$$g(\omega, k) = \frac{\omega_c(k)\omega_p^2(k)}{\omega(\omega_c^2(k) - \omega^2)}. \tag{B3}$$

Notice we have added nonlocal (momentum-dependent) corrections to both the plasma ω_p and cyclotron ω_c frequencies. As we will see, nonlocality is imperative to describe a topologically nontrivial phase. In terms of coupling matrices $\mathcal{C}$, the permittivity tensor can be expressed as

$$\varepsilon_{ij} = \delta_{ij} - \frac{[\mathcal{C}_+]_{il}[\mathcal{C}_+]^l_j}{\omega(\omega - \omega_c)} - \frac{[\mathcal{C}_-]_{il}[\mathcal{C}_-]^l_j}{\omega(\omega + \omega_c)}, \tag{B4}$$

where repeated indices imply summation and,

$$[\mathcal{C}_\pm]_{ij} = \frac{\omega_p}{2}(\delta_{ij} \pm i\epsilon_{ij}). \tag{B5}$$

The corresponding Hamiltonian $\omega u = Hu$ governing the total light-matter interaction is therefore

$$H = \begin{bmatrix} \mathcal{H}_0 & \mathcal{C}_+ & \mathcal{C}_- \\ \mathcal{C}_+ & \omega_c & 0 \\ \mathcal{C}_- & 0 & -\omega_c \end{bmatrix}, \quad u = \begin{bmatrix} f \\ \psi_+ \\ \psi_- \end{bmatrix}, \tag{B6}$$

where $\psi_\pm$ are the positive and negative energy matter oscillations. To be properly regularized, the nonlocaity (spatial dispersion) must be at least quadratic in k,

$$\omega_p(k) = \omega_{p0} + \omega_{p2}k^2, \quad \omega_c(k) = \omega_{c0} + \omega_{c2}k^2. \tag{B7}$$

Physically, the quadratic nonlocality arises from high-momentum corrections to the effective mass, since the electronic bands are not perfectly parabolic,

$$\frac{1}{M^*} = \frac{1}{\hbar^2}\frac{\partial^2 E}{\partial k^2} = \frac{1}{M_0} + \frac{1}{M_2}(ka)^2 + \cdots, \tag{B8}$$

which gives

$$\omega_{c0} = \frac{eB_0}{M_0}, \quad \omega_{c2} = \frac{eB_0}{M_2}a^2. \tag{B9}$$

a is the lattice constant in this case. Inserting into the wave equation, we obtain the dispersion relation

$$\omega^2\left(\varepsilon - \frac{g^2}{\varepsilon}\right) = k^2, \tag{B10}$$

which has two (positive energy) eigenmode branches,

$$\omega_\pm^2 = \frac{1}{2}\left[2\omega_p^2 + \omega_c^2 + k^2 \pm \sqrt{4\omega_p^2\omega_c^2 + \left(\omega_c^2 - k^2\right)^2}\right]. \tag{B11}$$

After a bit of work, it can be shown that the Chern number for each band is determined by the spin eigenvalues at $k_i = 0$ and $k_i = \infty$,

$$C_\pm = m_\pm(0) - m_\pm(\infty) = \mp[\mathrm{sgn}(\omega_{c0}) - \mathrm{sgn}(\omega_{c2})]. \tag{B12}$$

Alternatively, the Chern number can be expressed in terms of the relative sign of the effective masses, M_0 and M_2, and the applied magnetic field B_0,

$$C_\pm = \mp[\mathrm{sgn}(M_0) - \mathrm{sgn}(M_2)]\mathrm{sgn}(B_0). \tag{B13}$$

If the cyclotron frequency *switches sign* with momentum $\omega_{c0}\omega_{c2} < 0$, the topological phase is nontrivial $|C_\pm| = 2$. This implies there is an inflection point in the electronic band, $1/M^* = \partial^2 E/\partial k^2 = 0$, such that the curvature changes. More precisely, if there are an *odd* number of inflection points, the curvature changes an odd number of times, which always produces a nontrivial phase $|C_\pm| = 2$.

[1] M. Z. Hasan and C. L. Kane, Colloquium: Topological insulators, Rev. Mod. Phys. **82**, 3045 (2010).

[2] S. Ryu, A. P. Schnyder, A. Furusaki, and A. W. W. Ludwig, Topological insulators and superconductors: Tenfold way and dimensional hierarchy, New J. Phys. **12**, 065010 (2010).

[3] F. D. M. Haldane, Model for a Quantum Hall Effect without Landau Levels: Condensed-Matter Realization of the "Parity Anomaly", Phys. Rev. Lett. **61**, 2015 (1988).

[4] D. Jaksch and P. Zoller, Creation of effective magnetic fields in optical lattices: The Hofstadter butterfly for cold neutral atoms, New J. Phys. **5**, 56 (2003).

[5] J. Koch, A. A. Houck, K. L. Hur, and S. M. Girvin, Time-reversal-symmetry breaking in circuit-QED-based photon lattices, Phys. Rev. A **82**, 043811 (2010).

[6] G. Jotzu, M. Messer, R. Desbuquois, M. Lebrat, T. Uehlinger, D. Greif, and T. Esslinger, Experimental realization of the topological Haldane model with ultracold fermions, Nature (London) **515**, 237 (2014).

[7] B. A. Bernevig and T. L. Hughes, *Topological Insulators and Topological Superconductors* (Princeton University Press, Princeton, NJ, 2013).

[8] C. L. Kane and E. J. Mele, Quantum Spin Hall Effect in Graphene, Phys. Rev. Lett. **95**, 226801 (2005).

[9] B. A. Bernevig, T. L. Hughes, and S.-C. Zhang, Quantum spin Hall effect and topological phase transition in HgTe quantum wells, Science **314**, 1757 (2006).

[10] J. Maciejko, T. L. Hughes, and S.-C. Zhang, The quantum spin Hall effect, Annu. Rev. Condens. Matter Phys. **2**, 31 (2011).

[11] K. v. Klitzing, G. Dorda, and M. Pepper, New Method for High-Accuracy Determination of the Fine-Structure Constant Based on Quantized Hall Resistance, Phys. Rev. Lett. **45**, 494 (1980).

[12] R. B. Laughlin, Quantized Hall conductivity in two dimensions, Phys. Rev. B **23**, 5632 (1981).

[13] D. J. Thouless, M. Kohmoto, M. P. Nightingale, and M. den Nijs, Quantized Hall Conductance in a Two-Dimensional Periodic Potential, Phys. Rev. Lett. **49**, 405 (1982).

[14] Xie Chen, Zheng-Xin Liu, and Xiao-Gang Wen, Two-dimensional symmetry-protected topological orders and their protected gapless edge excitations, Phys. Rev. B **84**, 235141 (2011).

[15] Xie Chen, Zheng-Cheng Gu, Zheng-Xin Liu, and Xiao-Gang Wen, Symmetry-protected topological orders in interacting bosonic systems, Science **338**, 1604 (2012).

[16] Yuan-Ming Lu and A. Vishwanath, Theory and classification of interacting integer topological phases in two dimensions: A Chern-Simons approach, Phys. Rev. B **86**, 125119 (2012).

[17] A. Vishwanath and T. Senthil, Physics of Three-Dimensional Bosonic Topological Insulators: Surface-Deconfined Criticality and Quantized Magnetoelectric Effect, Phys. Rev. X **3**, 011016 (2013).

[18] M. A. Metlitski, C. L. Kane, and M. P. A. Fisher, Bosonic topological insulator in three dimensions and the statistical Witten effect, Phys. Rev. B **88**, 035131 (2013).

[19] T. Senthil and M. Levin, Integer Quantum Hall Effect for Bosons, Phys. Rev. Lett. **110**, 046801 (2013).

[20] Zeren Lin and Zhirong Liu, Spin-1 Dirac-Weyl fermions protected by bipartite symmetry, J. Chem. Phys. **143**, 214109 (2015).

[21] Tian Lan, Liang Kong, and Xiao-Gang Wen, Theory of (2+1)-dimensional fermionic topological orders and fermionic/bosonic topological orders with symmetries, Phys. Rev. B **94**, 155113 (2016).

[22] Tiantian Zhang, Zhida Song, A. Alexandradinata, Hongming Weng, Chen Fang, Ling Lu, and Zhong Fang, Double-Weyl Phonons in Transition-Metal Monosilicides, Phys. Rev. Lett. **120**, 016401 (2018).

[23] Y. Ikebe, T. Morimoto, R. Masutomi, T. Okamoto, H. Aoki, and R. Shimano, Optical Hall Effect in the Integer Quantum Hall Regime, Phys. Rev. Lett. **104**, 256802 (2010).

[24] Yisong Zheng and Tsuneya Ando, Hall conductivity of a two-dimensional graphite system, Phys. Rev. B **65**, 245420 (2002).

[25] T. Van Mechelen and Z. Jacob, Quantum gyroelectric effect:

Photon spin-1 quantization in continuum topological bosonic phases, Phys. Rev. A **98**, 023842 (2018).
[26] T. Van Mechelen and Z. Jacob, Photonic Dirac monopoles and skyrmions: Spin-1 quantization, Opt. Mater. Express **9**, 95 (2019).
[27] T. Van Mechelen and Z. Jacob, Unidirectional Maxwellian spin waves, arXiv:1903.09278.
[28] J. Preskill, Magnetic monopoles, Annu. Rev. Nucl. Part. Sci. **34**, 461 (1984).
[29] G. V. Dunne, Aspects of Chern-Simons theory, in *Aspects Topologiques de la Physique en Basse Dimension. Topological Aspects of Low Dimensional Systems*, edited by A. Comtet, T. Jolicœur, S. Ouvry, and F. David (Springer, Berlin/Heidelberg, 1999), pp. 177–263.
[30] D. Boyanovsky, R. Blankenbecler, and R. Yahalom, Physical origin of topological mass in 2 + 1 dimensions, Nucl. Phys. B **270**, 483 (1986).
[31] S. A. R. Horsley, Topology and the optical Dirac equation, Phys. Rev. A **98**, 043837 (2018).
[32] S. Raghu and F. D. M. Haldane, Analogs of Quantum-Hall-effect edge states in photonic crystals, Phys. Rev. A **78**, 033834 (2008).
[33] F. D. M. Haldane and S. Raghu, Possible Realization of Directional Optical Waveguides in Photonic Crystals with Broken Time-Reversal Symmetry, Phys. Rev. Lett. **100**, 013904 (2008).
[34] Zheng Wang, Yidong Chong, J. D. Joannopoulos, and M. Soljacic, Observation of unidirectional backscattering-immune topological electromagnetic states, Nature (London) **461**, 772 (2009).
[35] Zheng Wang and Shanhui Fan, Optical circulators in two-dimensional magneto-optical photonic crystals, Opt. Lett. **30**, 1989 (2005).
[36] Ling Lu, Liang Fu, J. D. Joannopoulos, and M. Soljacic, Weyl points and line nodes in gyroid photonic crystals, Nat. Photonics **7**, 294 (2013).
[37] M. Hafezi, S. Mittal, J. Fan, A. Migdall, and J. M. Taylor, Imaging topological edge states in silicon photonics, Nat. Photonics **7**, 1001 (2013), .
[38] Zheng-Cheng Gu, Zhenghan Wang, and Xiao-Gang Wen, Classification of two-dimensional fermionic and bosonic topological orders, Phys. Rev. B **91**, 125149 (2015).
[39] T. Karzig, C.-E. Bardyn, N. H. Lindner, and G. Refael, Topological Polaritons, Phys. Rev. X **5**, 031001 (2015).
[40] Y. Hadad, V. Vitelli, and A. Alu, Solitons and propagating domain walls in topological resonator arrays, ACS Photonics **4**, 1974 (2017).
[41] G. De Nittis and M. Lein, Symmetry classification of topological photonic crystals, arXiv:1710.08104.
[42] N. H. Lindner, G. Refael, and V. Galitski, Floquet topological insulator in semiconductor quantum wells, Nat. Phys. **7**, 490 (2011).
[43] J. Cayssol, B. Dora, F. Simon, and R. Moessner, Floquet topological insulators, Physica Status Solidi (RRL) **7**, 101 (2013).
[44] M. C. Rechtsman, J. M. Zeuner, Yonatan Plotnik, Yaakov Lumer, D. Podolsky, F. Dreisow, S. Nolte, M. Segev, and A. Szameit, Photonic Floquet topological insulators, Nature (London) **496**, 196 (2013).
[45] A. B. Khanikaev and G. Shvets, Two-dimensional topological photonics, Nat. Photonics **11**, 763 (2017).
[46] A. Slobozhanyuk, S. H. Mousavi, Xiang Ni, D. Smirnova, Y. S. Kivshar, and A. B. Khanikaev, Three-dimensional all-dielectric photonic topological insulator, Nat. Photonics **11**, 130 (2017), article .
[47] Cheng He, Xiao-Chen Sun, Xiao-Ping Liu, Ming-Hui Lu, Yulin Chen, Liang Feng, and Yan-Feng Chen, Photonic topological insulator with broken time-reversal symmetry, Proc. Natl. Acad. Sci. USA **113**, 4924 (2016).
[48] S. B. Glybovski, S. A. Tretyakov, P. A. Belov, Y. S. Kivshar, and C. R. Simovski, Metasurfaces: From microwaves to visible, Phys. Rep. **634**, 1 (2016), .
[49] I. V. Lindell and A. H. Sihvola, Realization of the PEMC boundary, IEEE Trans. Antennas Propag. **53**, 3012 (2005).
[50] R. Alaee, M. Farhat, C. Rockstuhl, and F. Lederer, A perfect absorber made of a graphene micro-ribbon metamaterial, Opt. Express **20**, 28017 (2012).
[51] N. Papasimakis, Zhiqiang Luo, Ze Xiang Shen, Francesco De Angelis, Enzo Di Fabrizio, A. E. Nikolaenko, and N. I. Zheludev, Graphene in a photonic metamaterial, Opt. Express **18**, 8353 (2010).
[52] Junfei Li, Chen Shen, Ana Díaz-Rubio, S. A. Tretyakov, and S. A. Cummer, Systematic design and experimental demonstration of bianisotropic metasurfaces for scattering-free manipulation of acoustic wavefronts, Nat. Commun. **9**, 1342 (2018).
[53] Yu Guo, Meng Xiao, and Shanhui Fan, Topologically Protected Complete Polarization Conversion, Phys. Rev. Lett. **119**, 167401 (2017).
[54] Kun Ding, Guancong Ma, Meng Xiao, Z. Q. Zhang, and C. T. Chan, Emergence, Coalescence, and Topological Properties of Multiple Exceptional Points and their Experimental Realization, Phys. Rev. X **6**, 021007 (2016).
[55] M. G. Silveirinha, Chern invariants for continuous media, Phys. Rev. B **92**, 125153 (2015).
[56] Wenlong Gao, M. Lawrence, Biao Yang, Fu Liu, Fengzhou Fang, Benjamin Béri, Jensen Li, and Shuang Zhang, Topological Photonic Phase in Chiral Hyperbolic Metamaterials, Phys. Rev. Lett. **114**, 037402 (2015).
[57] D. Jin, Ling Lu, Zhong Wang, Chen Fang, J. D. Joannopoulos, M. Soljacic, Liang Fu, and N. X. Fang, Topological magnetoplasmon, Nat. Commun. **7**, 13486 EP (2016).
[58] S. A. Hassani Gangaraj, M. G. Silveirinha, and G. W. Hanson, Berry phase, Berry connection, and Chern number for a continuum bianisotropic material from a classical electromagnetics perspective, IEEE J. Multiscale Multiphys. Comput. Tech. **2**, 3 (2017).
[59] Li-kun Shi and J. C. W. Song, Plasmon Geometric Phase and Plasmon Hall Shift, Phys. Rev. X **8**, 021020 (2018).
[60] Iwo Bialynicki-Birula and Zofia Bialynicka-Birula, Berry's phase in the relativistic theory of spinning particles, Phys. Rev. D **35**, 2383 (1987).
[61] M. Stone, Berry phase and anomalous velocity of Weyl fermions and Maxwell photons, Int. J. Mod. Phys. B **30**, 1550249 (2016).
[62] M. Stone, Topology, spin, and light, Science **348**, 1432 (2015).
[63] O. E. Gawhary, T. Van Mechelen, and H. P. Urbach, Role of Radial Charges on the Angular Momentum of Electromagnetic Fields: Spin-3/2 Light, Phys. Rev. Lett. **121**, 123202 (2018).
[64] J. Hubbard, The dielectric theory of electronic interactions in solids, Proc. Phys. Soc., A **68**, 976 (1955).

[65] D. S. Falk, Effect of the lattice on dielectric properties of an electron gas, Phys. Rev. **118**, 105 (1960).

[66] D. R. Penn, Wave-number-dependent dielectric function of semiconductors, Phys. Rev. **128**, 2093 (1962).

[67] L. D. Landau, J. S. Bell, M. J. Kearsley, L. P. Pitaevskii, E. M. Lifshitz, and J. B. Sykes, *Electrodynamics of Continuous Media*, Landau and Lifshitz Course of Theoretical Physics Vol. 8 (Elsevier, New York, 2013).

[68] V. M. Agranovich and V. Ginzburg, *Crystal Optics with Spatial Dispersion, and Excitons* (Springer Science & Business Media, New York, 2013), Vol. 42.

[69] Liang Fu, Topological Crystalline Insulators, Phys. Rev. Lett. **106**, 106802 (2011).

[70] T. L. Hughes, E. Prodan, and B. A. Bernevig, Inversion-symmetric topological insulators, Phys. Rev. B **83**, 245132 (2011).

[71] R.-J. Slager, A. Mesaros, V. Juricic, and J. Zaanen, The space group classification of topological band-insulators, Nat. Phys. **9**, 98 (2012).

[72] C. Fang, M. J. Gilbert, and B. A. Bernevig, Bulk topological invariants in noninteracting point group symmetric insulators, Phys. Rev. B **86**, 115112 (2012).

[73] J. Kruthoff, J. de Boer, J. van Wezel, C. L. Kane, and R.-J. Slager, Topological Classification of Crystalline Insulators through Band Structure Combinatorics, Phys. Rev. X **7**, 041069 (2017).

[74] B. Bradlyn, L. Elcoro, J. Cano, M. G. Vergniory, Zhijun Wang, C. Felser, M. I. Aroyo, and B. A. Bernevig, Topological quantum chemistry, Nature (London) **547**, 298 (2017).

[75] Hao Song, Sheng-Jie Huang, Liang Fu, and M. Hermele, Topological Phases Protected by Point Group Symmetry, Phys. Rev. X **7**, 011020 (2017).

[76] T. A. Sedrakyan, V. M. Galitski, and A. Kamenev, Topological spin ordering via Chern-Simons superconductivity, Phys. Rev. B **95**, 094511 (2017).

[77] Hoi Chun Po, A. Vishwanath, and H. Watanabe, Symmetry-based indicators of band topology in the 230 space groups, Nat. Commun. **8**, 50 (2017).

[78] R. Thorngren and D. V. Else, Gauging Spatial Symmetries and the Classification of Topological Crystalline Phases, Phys. Rev. X **8**, 011040 (2018).

[79] A. Matsugatani, Y. Ishiguro, K. Shiozaki, and H. Watanabe, Universal Relation among the Many-Body Chern Number, Rotation Symmetry, and Filling, Phys. Rev. Lett. **120**, 096601 (2018).

[80] H. Watanabe, H. C. Po, and A. Vishwanath, Structure and topology of band structures in the 1651 magnetic space groups, Sci. Adv. **4**, eaat8685 (2018).

[81] B. Bradlyn, J. Cano, Zhijun Wang, M. G. Vergniory, C. Felser, R. J. Cava, and B. A. Bernevig, Beyond Dirac and Weyl fermions: Unconventional quasiparticles in conventional crystals, Science **353**, aaf5037 (2016).

[82] Yan-Qing Zhu, Dan-Wei Zhang, Hui Yan, Ding-Yu Xing, and Shi-Liang Zhu, Emergent pseudospin-1 Maxwell fermions with a threefold degeneracy in optical lattices, Phys. Rev. A **96**, 033634 (2017).

[83] Haiping Hu and Chuanwei Zhang, Spin-1 topological monopoles in the parameter space of ultracold atoms, Phys. Rev. A **98**, 013627 (2018).

[84] Haiping Hu, Junpeng Hou, Fan Zhang, and Chuanwei Zhang, Topological Triply Degenerate Points Induced by Spin-Tensor-Momentum Couplings, Phys. Rev. Lett. **120**, 240401 (2018).

[85] I. C. Fulga, L. Fallani, and M. Burrello, Geometrically protected triple-point crossings in an optical lattice, Phys. Rev. B **97**, 121402(R) (2018).

[86] Xinsheng Tan, Dan-Wei Zhang, Qiang Liu, Guangming Xue, Hai-Feng Yu, Yan-Qing Zhu, Hui Yan, Shi-Liang Zhu, and Yang Yu, Topological Maxwell Metal Bands in a Superconducting Qutrit, Phys. Rev. Lett. **120**, 130503 (2018).

[87] T. Van Mechelen and Z. Jacob, Dirac-Maxwell correspondence: Spin-1 bosonic topological insulator, in *Proceedings of the 2018 Conference on Lasers and Electro-Optics (CLEO)* (IEEE, San Jose, CA, 2018), pp. 1–2.

[88] Xiaobo Yin, Ziliang Ye, Junsuk Rho, Yuan Wang, and Xiang Zhang, Photonic spin Hall effect at metasurfaces, Science **339**, 1405 (2013).

[89] T. V. Mechelen and Z. Jacob, Universal spin-momentum locking of evanescent waves, Optica **3**, 118 (2016).

[90] F. Kalhor, T. Thundat, and Z. Jacob, Universal spin-momentum locked optical forces, Appl. Phys. Lett. **108**, 061102 (2016).

[91] S. Pendharker, F. Kalhor, T. V. Mechelen, S. Jahani, N. Nazemifard, T. Thundat, and Z. Jacob, Spin photonic forces in non-reciprocal waveguides, Opt. Express **26**, 23898 (2018).

[92] K. Y. Bliokh, D. Smirnova, and F. Nori, Quantum spin Hall effect of light, Science **348**, 1448 (2015).

[93] M. Born and K. Huang, *Dynamical Theory of Crystal Lattices* (Clarendon, Oxford, 1954).

[94] A. F. J. Levi, The Lorentz oscillator model, in *Essential Classical Mechanics for Device Physics* (Morgan & Claypool, San Rafael, CA, 2016), pp. 5-1 to 5-21.

[95] D. Hestenes, Point groups and space groups in geometric algebra, in *Applications of Geometric Algebra in Computer Science and Engineering*, edited by Leo Dorst, Chris Doran, and Joan Lasenby (Birkhäuser Boston, Boston, MA, 2002), pp. 3–34.

[96] John Frederick Nye, *Physical Properties of Crystals: Their Representation by Tensors and Matrices* (Oxford University Press, New York, 1985).